Frank Hanekamhaug

Dynamic Analysis of a Francis Turbine

June 2019

Master's thesis

2019

Master's thesis

Frank Hanekamhaug

NTNU
Norwegian University of
Science and Technology
Faculty of Engineering
Department of Mechanical and Industrial Engineering

NTNU
Norwegian University of
Science and Technology

NTNU
Norwegian University of
Science and Technology

Dynamic Analysis of a Francis Turbine

Frank Hanekamhaug

Sammendrag

Francisturbiner er velkjente installasjoner i norske vannkraftverk. De dynamiske egenskapene til en Francisturbin påvirkes signifikant av miljøet den opererer i, det er derfor et stort ønske å forstå samspillet mellom turbin og vann bedre for å sikre stabil kraftproduksjon. Denne masteroppgaven betrakter en forenklet modell av en Francisturbin, modellen er nedsenket i vann og blir utsatt for en støtkraft. Det ble utført to forskjellige analysemetoder på modellen, begge utført i Abaqus explicit dynamics. En akustisk-struktur koblet analyse og en Euler-Lagrange koblet analyse. Det er lagt vekt på oppsett og resultater fra simuleringene for å finne den best egnede metoden for denne type problemer. Metodene er svært ulike, og det er derfor utfordrende å tilegne identiske forutsetninger i simuleringene.

Den akustisk-struktur koblede analysen viste seg som en svært pålitelig metode. Tolkning av energimengdene indikerte en optimal simulering. Et dempingsforhold ble utregnet fra forskyvningens amplituder, og grunnet fravær av viskositet i de akustiske elementene ble dempingforholdet lavt. Den Euler-Lagrange koblete analysen var tvetydig i henhold til pålitelighet. Energimengdene tilstede i simuleringen indikerte en ikke-optimalisert simulering, og nødvendige tiltak er derfor anbefalt. Dempingsforholdet ble utregnet fra forskyvningens amplituder, og det ble funnet et høyere dempingsforhold enn for den akustisk-struktur koblede analysen.

Euler-Lagrange metoden ble ansett best egnet, selv med indikasjonene på en ikke-optimalisert simulering. Metoden viser seg å være allsidig og har mulighet for å implementeres i mer avanserte problemer.

Preface

This master thesis is an original product of Frank Hanekamhaug, and is written as a fulfilment of the Master of Science degree at Norwegian University of Science and Technology. The thesis contains theoretical and numerical approaches to analyse the influence water can have on a Francis turbine.

Associate professor Bjørn Haugen at the Department of Mechanical and Industrial Engineering has been supervisor during the process of writing this master thesis.

Acknowledgment

My sincere gratitude to supervisor Bjørn Haugen for excellent theoretical, decision taking and motivational support through the process of this master thesis.

I would also like to thank my family at home, Linn and Herman for keeping up with me during the process of writing this master thesis, and especially my son for giving me reasons to unwind.

The continuous support from my parents have also been crucial for finally finishing my degree at the Norwegian University of Science and Technology.

F.H.

Abstract

Using software to simulate behavior of structures and components has been an important tool in engineering for the last decades. The demand for more complex applications has arisen and the software has developed simultaneously, thanks to the exponentially growth of faster computers. This implies that one has the possibility to do what was previously unthinkable, on a regular computer. Numerical analysis of complex geometries such as a Francis turbine interacting with a fluid are still reserved high-end hardware, and not applicable to laptops. Simplified geometries are therefore considered to keep simulation time at an acceptable level.

Fluid-structure interaction (FSI) couples the structural dynamics with the fluid dynamics and letting them interact with each other. From a two-way coupling it is also possible the separately examine the behavior, due to the fact that in some cases the fluid dynamics are of interest and in other cases it is the structural dynamics which are of interest.
For the situation with an immersed steel structure with a surrounding fluid and with only interest of the dynamics of the steel structure, the problem can be simulated in different ways. This master thesis contains a coupled acoustic-structure (CAS) numerical analysis and a coupled Eulerian-Lagrangian (CEL) numerical analysis. The simulations are executed in Abaqus 2017 software and primary focus will be at the structural response and energies.

Comparison of the different approaches indicates that the CAS technique is slightly more accurate from a numerical point of view, has easier setup and requires less processor power. Nevertheless the CAS technique is not that versatile and unable to simulate real situations, due to the use of acoustic elements. The CEL technique offers more input parameters and easy access for changing the parameters of the fluid. A complete overview of the fluid flow is also available. Complex setup, no possibility for re-meshing and a need for using small elements in the Eulerian domain are the drawbacks.

Contents

List of Tables

List of Figures

Abbreviations and Nomenclature

Abbreviations

ALE   Arbitrary Lagrangian Eulerian

CAS   Coupled acoustic structure

CEL   Coupled Eulerian Lagrangian

EVF   Eulerian volume fraction

FSI   Fluid structure interaction

Nomenclature

∇	Gradient variable	$length^{-1}$
$\boldsymbol{\sigma}$	Stress tensor	$\frac{N}{mm^2}$
$\tilde{\nabla}$	Differential operator	$length^{-1}$
ϵ_S	Strain steel	$-$
η	Viscosity coefficient	$\frac{Ns}{mm^2}$
γ_S	Shear strain steel	$-$
κ	Viscosity coefficient [dynamic]	$\frac{Ns}{mm^2}$
λ	Lamè parameter	$\frac{N}{mm^2}$
$\mathbf{b}_F$	Body force fluid	$\frac{N}{mm^3}$
$\mathbf{b}_S$	Body force structure	$\frac{N}{mm^3}$
$\mathbf{D}_S$	Constitutive matrix steel	$\frac{N}{mm^2}$

$\mathbf{g}_F$	Heat flux vector	$\frac{J}{smm^2}$
$\mathbf{k}$	Conductivity tensor	$\frac{J}{smmK^{-1}}$
$\mathbf{n}$	Unit normal	$-$
$\mathbf{q}_S$	Inertia force	$\frac{N}{mm^3}$
$\mathbf{t}$	Unit tangential	$-$
$\mathbf{t}_S$	Traction vector	$\frac{N}{mm^2}$
$\mathbf{u}_F$	Displacement fluid	mm
$\mathbf{u}_S$	Displacement structure	mm
$\mathbf{v}_F$	Velocity fluid	$\frac{mm}{s}$
$\mathbf{w}_S$	Weight function	$-$
$\mathbf{D}_F$	Velocity strain tensor fluid	s^{-1}
μ	Lamè parameter	$\frac{N}{mm^2}$
ν	Poisson ratio	$-$
ρ_0	Static density fluid	$\frac{ton}{mm^3}$
ρ_F	Dynamic density fluid	$\frac{ton}{mm^3}$
ρ_S	Density structure	$\frac{ton}{mm^3}$
$\tilde{\mathbf{v}}_F$	Velocity mesh	$\frac{mm}{s}$
c_0	Speed of sound in acoustic fluid	$\frac{mm}{s}$
c_1	Speed of sound in Eulerian fluid	$\frac{mm}{s}$
E	Elastic modulus	$\frac{N}{mm^2}$
K_F	Bulk modulus	$\frac{N}{mm^2}$

p_F	Dynamic pressure	$\frac{N}{mm^2}$
q_F	Added fluid mass per unit volume	$\frac{ton}{mm^3}$
δ	Logarithmic decrement	$-$
ζ	Damping ratio	$-$
e	Specific internal energy	$\frac{J}{ton}$
g_F	Rate of heat per unit volume	$\frac{J}{smm^3}$
T	Temperature	K

1 Introduction

The dynamic behavior of structures and fluids interacting with each other are a common challenge in engineering. The underlying theories of the domains are considerable different and must be united in a coupled analysis. The approach for a fluid-structure interactions (FSI) can be done in a variety of ways, depending on what is of interest.
In order to investigate the dynamics of a steel structure immersed in a fluid it can be simulated with numerical analysis. This master thesis will study a coupled acoustic-structure (CAS) simulation and a coupled Eulerian-Lagrangian (CEL) simulation. The diverse approach in the simulation procedures posts a question about what is most realistic.

In a CAS analysis problem there has been conducted several previous studies by A.Craggs [1],G.C Everstime [2] and by Sandberg [3] whose articles are presented in the book "Computational Aspects of Structural Acoustics and Vibration" [4], along with other articles of importance. In the CAS finite element analysis the meshes are coupled node to node at the boundary of each domain, and therefore can large mesh displacements be present. Gravity load or gravity fields are also not applicable in the traditional way when using the acoustic elements. If this is desired in an acoustic analysis it must be specified as an impedance condition [5]. Impedance is not specified for this CAS analysis.

The CEL approach differs from the CAS approach, in the way that the Eulerian mesh is fixed in space and the material flows through the elements. Previous studies on the Eulerian-Lagrangian approach are conducted by Benson [6] [7] and Bathe [8]. This approach has now become a common implementation in most numerical software tools. A drawback with the CEL method is the complexity it induces when defining the contact at the boundary between the two regions and a possible loss of accuracy due to the use of Eulerian volume fraction (EVF) tool.

The choice of algorithm, either the CAS or the CEL, is a very complex problem for the user and is very dependent on the problem definition. Using simplified geometries as a representation for the complex geometry of a Francis turbine and investigating the numerical results achieved, the most suitable numerical analysis approach for this type of problem is to be designated.

The use of simplified geometries are done to keep computational costs reasonable. In the future the results of the simplified geometries can be transferred to more complex geometries such as a Francis turbine, and hopefully also save computation time by choosing the most appropriate method. This master thesis seeks to investigate obtained numerical results such as displacements, velocities and energies when the steel structure is immersed in a fluid and subjected to an instantaneous force of 10 N. The damping ratios will be calculated on basis of the displacements and a user evaluation of the analysis setup will also be considered when finding the most suitable approach.

The motivation writing this master thesis is that the results obtained from the simple models can be transferred to more complex models and save computational costs and time. A chronological reading is advised as a traditional thesis structure is chosen, starting with theory, numerical methods, results and discussion, conclusion and ending with recommendations for further work.

All numerical analysis are done in Abaqus software, version 6.17.

2 Theory

2.1 Acoustic-structure theory

Dynamics of different materials interacting with each other are a complex matter when using analytical expressions and dealing with multiple dimensions. In an acoustic-structure analysis both materials are treated as Lagrangian, i.e the nodes are fixed in the material and follow the material deformation. In the Lagrangian theory, each element contains 100% of one single material, so that the boundary of a material coincides with the element boundary [9]. For Lagrangian problems and in possession of computers, the complex analytical equations are discretized in time and space and applied finite element formulations. This enables the use of numerical analysis tools on the computer. The work of Craggs [1], Zienkiwics[10], Sandberg [4] together with familiar curriculum from Fish [11] and Ottosen [12] are considered throughout the acoustic-structure finite element (FE) derivation. The main inspirational source is from the work of Sandberg.

2.1.1 Governing equations

The governing equations for the structural domain, acoustic domain and the coupled system domain are presented in equations 2.1, 2.2 and 2.3.

The notation for the structural domain in equation 2.1 are as followed, $\boldsymbol{\sigma}_S$ is the stress tensor, $\mathbf{b}_S$ is the body force and $\rho_S \frac{\partial^2 \mathbf{u}_S}{\partial t^2} = \mathbf{q}_S$ is the inertia force, where ρ_S is the density and $\mathbf{u}_S$ is the displacement. $\tilde{\nabla}$ is the differential operator. For the acoustic domain, in equation 2.2 the non homogeneous wave equation is expressed with notations, p_F is the dynamic pressure, c_0 is the speed of sound in the acoustic fluid, ∇ is a gradient variable and q_F is the added fluid mass per unit volume. The coupling equations represented in equation 2.3 guarantees continuity between the structural and acoustic domain, and the notations are as followed, $u_S|_n$ is the displacement in normal direction for the structure and $u_F|_n$ is the displacement in normal direction for the fluid. The $\sigma_S|_n$ is the stress in normal directions for the structure and p_F is the acoustic fluid pressure.

3

$$\begin{cases} \tilde{\nabla}^T \boldsymbol{\sigma}_S + \mathbf{b}_S = \rho_S \frac{\partial^2 \mathbf{u}_s}{\partial t^2} = \mathbf{q}_S & \Omega_S \\ +B.C \end{cases} \tag{2.1}$$

$$\begin{cases} \frac{\partial^2 p_F}{\partial^2 t} - c_0^2 \nabla^2 p_F = c_0^2 \frac{\partial q_F}{\partial t} & \Omega_F \\ +B.C \end{cases} \tag{2.2}$$

$$\begin{cases} u_S|_n = u_F|_n & \Omega_{FS} \\ \sigma_S|_n = -p_F & \Omega_{FS} \end{cases} \tag{2.3}$$

4

2.1.2 FE formulation for structural domain

Given the vector form of the displacement and body force they are expressed as in equation 2.4.

$$\mathbf{u}_s = \begin{bmatrix} u_1^S \\ u_3^S \\ u_3^S \end{bmatrix} \quad \text{and} \quad \mathbf{b}_s = \begin{bmatrix} b_1^S \\ b_3^S \\ b_3^S \end{bmatrix} \tag{2.4}$$

Remembering the definition for the stress and strain, and expressing the differential operator $\tilde{\nabla}$ in matrix form in equation 2.5.

$$\tilde{\nabla} = \begin{bmatrix} \frac{\partial}{\partial x_1} & 0 & 0 \\ 0 & \frac{\partial}{\partial x_2} & 0 \\ 0 & 0 & \frac{\partial}{\partial x_3} \\ \frac{\partial}{\partial x_2} & \frac{\partial}{\partial x_1} & 0 \\ \frac{\partial}{\partial x_3} & 0 & \frac{\partial}{\partial x_1} \\ 0 & \frac{\partial}{\partial x_3} & \frac{\partial}{\partial x_2} \end{bmatrix} \tag{2.5}$$

The definition for the Green-Lagrange strain tensor $\mathbf{E}_S$ in equation 2.6 and the Cauchy stress tensor $\mathbf{S}_S$ in equation 2.7.

$$\mathbf{E}_S = \begin{bmatrix} \epsilon_{11}^S & \epsilon_{12}^S & \epsilon_{13}^S \\ \epsilon_{21}^S & \epsilon_{22}^S & \epsilon_{23}^S \\ \epsilon_{31}^S & \epsilon_{32}^S & \epsilon_{33}^S \end{bmatrix} \tag{2.6}$$

$$\mathbf{S}_S = \begin{bmatrix} \sigma_{11}^S & \sigma_{12}^S & \sigma_{13}^S \\ \sigma_{21}^S & \sigma_{22}^S & \sigma_{23}^S \\ \sigma_{31}^S & \sigma_{32}^S & \sigma_{33}^S \end{bmatrix} \tag{2.7}$$

Using infinitesimal strain theory $\epsilon_{ij} = \frac{1}{2}(u_{i,j} + u_{j,i})$, and utilizing the symmetry of the stress tensor matrix $\sigma_{12}^S = \sigma_{21}^S$, $\sigma_{13}^S = \sigma_{31}^S$ and $\sigma_{23}^S = \sigma_{32}^S$.

The strain components and the stress can also be expressed as in equation 2.8 and equation 2.9.

$$\epsilon_{ij} = \frac{1}{2}(u_{i,j} + u_{j,i}) = \begin{bmatrix} \frac{\partial u_1}{\partial x_1} & \frac{1}{2}\left(\frac{\partial u_1}{\partial x_2} + \frac{\partial u_2}{\partial x_1}\right) & \frac{1}{2}\left(\frac{\partial u_1}{\partial x_3} + \frac{\partial u_3}{\partial x_1}\right) \\ \frac{1}{2}\left(\frac{\partial u_2}{\partial x_1} + \frac{\partial u_1}{\partial x_2}\right) & \frac{\partial u_2}{\partial x_2} & \frac{1}{2}\left(\frac{\partial u_2}{\partial x_3} + \frac{\partial u_3}{\partial x_2}\right) \\ \frac{1}{2}\left(\frac{\partial u_3}{\partial x_1} + \frac{\partial u_1}{\partial x_3}\right) & \frac{1}{2}\left(\frac{\partial u_3}{\partial x_2} + \frac{\partial u_2}{\partial x_3}\right) & \frac{\partial u_3}{\partial x_3} \end{bmatrix} \tag{2.8}$$

$$\mathbf{S}_S = \begin{bmatrix} \sigma_{11}^S & \sigma_{12}^S & \sigma_{13}^S \\ \sigma_{12}^S & \sigma_{22}^S & \sigma_{23}^S \\ \sigma_{13}^S & \sigma_{23}^S & \sigma_{33}^S \end{bmatrix} \tag{2.9}$$

By using the theories, definitions and formulas, the strains and stresses can be expressed in simple 6×1 matrix notation shown in equation 2.10 and equation 2.11, where γ is the notation for the shear strain.

$$\tilde{\nabla}\mathbf{u}_S = \epsilon_S = \begin{bmatrix} \epsilon_{11}^S \\ \epsilon_{22}^S \\ \epsilon_{33}^S \\ \frac{1}{2}\gamma_{12}^S \\ \frac{1}{2}\gamma_{13}^S \\ \frac{1}{2}\gamma_{23}^S \end{bmatrix} \tag{2.10}$$

$$\boldsymbol{\sigma}_S = \begin{bmatrix} \sigma_{11}^S \\ \sigma_{22}^S \\ \sigma_{33}^S \\ \sigma_{12}^S \\ \sigma_{13}^S \\ \sigma_{23}^S \end{bmatrix} \tag{2.11}$$

The constitutive matrix relates the stresses to the strains using the material properties with the relation $\boldsymbol{\sigma}_S = \mathbf{D}_S \epsilon_S$. Given the Lamè parameters [13] in equation 2.12.

$$\lambda = \frac{\nu E}{(1+\nu)(1-2\nu)} \qquad \text{and} \qquad \mu = G = \frac{E}{2(1+\nu)} \tag{2.12}$$

The constitutive matrix for an isotropic material can be represented on the tidy form given in equation 2.13.

$$\mathbf{D}_S = \begin{bmatrix} \lambda+2\mu & \lambda & \lambda & 0 & 0 & 0 \\ 0 & \lambda+2\mu & \lambda & 0 & 0 & 0 \\ 0 & 0 & \lambda+2\mu & 0 & 0 & 0 \\ 0 & 0 & 0 & \mu & 0 & 0 \\ 0 & 0 & 0 & 0 & \mu & 0 \\ 0 & 0 & 0 & 0 & 0 & \mu \end{bmatrix} \tag{2.13}$$

The strong form of the structural equation 2.1 are then multiplied with a weight function $\mathbf{w}_S = [w_1\, w_2\, w_3]^T$ and then integrated. Applying Green-Gauss theorem [12] and introducing a surface traction vector $\mathbf{t}_S = \mathbf{S}_S \mathbf{n}_S$, where $\mathbf{t}_S$ is related to the Cauchy stress tensor and a unit normal vector $\mathbf{n}_S$. Then, finally the weak form for the structure can be expressed in equation 2.14.

$$\int_{\Omega_S} \mathbf{w}_S^T \rho_S \frac{\partial^2 \mathbf{u}_S}{\partial t^2} dV + \int_{\Omega_S} (\tilde{\nabla}\mathbf{w}_S)^T \boldsymbol{\sigma}_S dV - \int_{\partial\Omega_S} \mathbf{w}_S^T \mathbf{t}_S dS - \int_{\Omega_S} \mathbf{w}_S^T \mathbf{b}_S dV = 0 \tag{2.14}$$

Using polynomials for the elementwise approximation of the shape functions $\mathbf{N}_S$, now allowing a discretization the displacements, weight functions and strain with the relation in equation 2.15. Where $\mathbf{d}_S$ is the nodal displacement and $\mathbf{c}_S$ is the nodal weight.

$$\mathbf{u}_S = \mathbf{N}_S \mathbf{d}_S, \qquad \mathbf{w}_S = \mathbf{N}_S \mathbf{c}_S, \qquad \boldsymbol{\epsilon}_S = \tilde{\nabla}\mathbf{N}_S \mathbf{d}_S \tag{2.15}$$

Observing that $\mathbf{c}_S$ is a constant eliminated from the expression, the finite element formulation for the problem is shown in integral form in 2.16 and in compressed form in equation 2.17.

$$\underbrace{\int_{\Omega_S} \mathbf{N}_S^T \rho_S \mathbf{N}_S dV \ddot{\mathbf{d}}_S}_{\mathbf{M}_S} + \underbrace{\int_{\Omega_S} (\tilde{\nabla}\mathbf{N}_S)^T \mathbf{D}_S \tilde{\nabla}\mathbf{N}_S dV \mathbf{d}_S}_{\mathbf{K}_S} = \underbrace{\int_{\partial\Omega_S} \mathbf{N}_S^T \mathbf{t}_S dS}_{\mathbf{f}_a} + \underbrace{\int_{\Omega_S} \mathbf{N}_S^T \mathbf{b}_S dV}_{\mathbf{f}_b} \tag{2.16}$$

$$\mathbf{M}_S \ddot{\mathbf{d}}_S + \mathbf{K}_S \mathbf{d}_S = \mathbf{f}_a + \mathbf{f}_b \tag{2.17}$$

2.1.3 FE formulation for acoustic domain

The strong form of the governing acoustic equation 2.2 must also be rewritten into a more convenient weak form. For a compressible acoustic fluid the assumptions that it is inviscid, irrotational and undergoes small translations. The motion equation then becomes.

$$\rho_0 \frac{\partial^2 \mathbf{u}_F(t)}{\partial t^2} + \nabla p_F(t) = 0 \tag{2.18}$$

Continuity equation are as followed.

$$\frac{\partial \rho_F(t)}{\partial t} + \rho_0 \nabla \frac{\partial \mathbf{u}_F(t)}{\partial t} = q_F(t) \tag{2.19}$$

The constitutive equation relates the dynamic density to the dynamic pressure.

$$p_F(t) = c_0^2 \rho_F(t) \tag{2.20}$$

Notations for equation 2.18 to 2.20 are as followed, $\rho_F(t)$ is the dynamic density, $q_F(t)$ is the added fluid mass per unit volume, $\nabla = [\frac{\partial}{\partial x_1} \frac{\partial}{\partial x_2} \frac{\partial}{\partial x_3}]^T$ is a gradient variable, $\mathbf{u}_F(t)$ is the displacement and ρ_0 is static density. Also the relation equation for the speed of sound in the acoustic fluid are shown in equation 2.21, where K_F is the bulk modulus.

$$c_0 = \sqrt{\frac{K_F}{\rho_0}} \tag{2.21}$$

Now with possession of equations 2.18, 2.19 and 2.20 the wave equation can be obtained by differentiating 2.19 once with respect to time, then differentiating 2.20 twice with respect to time. Using 2.18 for substitution and multiplying by c_0^2 to move it from the denominator to the numerator. The strong form of the homogeneous wave equation then becomes as in equation 2.22 i.e the same as earlier presented in equation 2.2.

$$\frac{\partial^2 p_F}{\partial^2 t} - c_0^2 \nabla^2 p_F = c_0^2 \frac{\partial q_F}{\partial t} \tag{2.22}$$

To arrive to the more convenient weak form, equation 2.22 is multiplied with a weight function w_F, integrated and applied the Gauss-Green's theorem. The weak formulation of the equation then becomes.

$$\int_{\Omega_F} w_F \frac{\partial^2 p_F}{\partial t^2} dV + c_0^2 \int_{\Omega_F} \nabla w_F \nabla p_F dV - c_0^2 \int_{\partial\Omega_F} w_F \nabla p_F \mathbf{n}_F dA - c_0^2 \int_{\Omega_F} w_F \frac{\partial q_F}{\partial t} dV = 0 \tag{2.23}$$

Introducing the polynomial shape functions $\mathbf{N}_F$, and $\mathbf{p}_F$ for the nodal pressures and $\mathbf{c}_F$ for the nodal weights.

$$p_F = \mathbf{N}_F \mathbf{p}_F \qquad w_F = \mathbf{N}_F \mathbf{c}_F \tag{2.24}$$

Integral form the finite element formulation for the acoustic domain then becomes.

$$\underbrace{\int_{\Omega_F} \mathbf{N}_F^T \mathbf{N}_F dV}_{\mathbf{M}_F} \ddot{\mathbf{p}}_F + \underbrace{c_0^2 \int_{\Omega_F} (\nabla \mathbf{N}_F)^T \nabla \mathbf{N}_F dV}_{\mathbf{K}_F} \mathbf{p}_F = \underbrace{c_0^2 \int_{\partial\Omega_F} \mathbf{N}_F^T \nabla p_F \mathbf{n}_F dS}_{\mathbf{f}_c} + \underbrace{c_0^2 \int_{\Omega_F} \mathbf{N}_F^T \frac{\partial q_F}{\partial t} dV}_{\mathbf{f}_q} \tag{2.25}$$

Written in a compact form the equations for the acoustic fluid can be expressed on the general form.

$$\mathbf{M}_F \ddot{\mathbf{p}}_F + \mathbf{K}_F \mathbf{p}_F = \mathbf{f}_c + \mathbf{f}_q \tag{2.26}$$

2.1.4 FE formulation for the coupled system

The interface between the structure and fluid domain must be coupled in a way that ensures continuity. A normal vector $\mathbf{n} = -\mathbf{n}_S = \mathbf{n}_F$ is suggested so that the dynamics of different domains follow each other. For the displacement and pressure this becomes.

$$\mathbf{u}_S\mathbf{n}|_{\partial\Omega_{FS}} = \mathbf{u}_F\mathbf{n}|_{\partial\Omega_{FS}} \tag{2.27}$$

$$\sigma_S|_n = p_F \tag{2.28}$$

The structural stress tensor $\mathbf{S}_S$ at the boundary $\partial\Omega_{FS}$ must be expressed in desired directions.

$$\mathbf{S}_S = -p_F \begin{bmatrix} 1 & 0 & 0 \\ 0 & 1 & 0 \\ 0 & 0 & 1 \end{bmatrix} \tag{2.29}$$

Then $\mathbf{f}_a$ from equation 2.17 in the structural domain is allowed to be rewritten in terms of the coupling domain $\partial\Omega_{SF}$.

Remembering $\mathbf{n} = -\mathbf{n}_S$, so the force on the structure is formulated as acoustic medium pressure.

$$\mathbf{f}_a = \int_{\partial\Omega_{FS}} \mathbf{N}_S^T(-p_F) \begin{bmatrix} 1 & 0 & 0 \\ 0 & 1 & 0 \\ 0 & 0 & 1 \end{bmatrix} \mathbf{n}_S dS = \int_{\partial\Omega_{FS}} \mathbf{N}_S^T \mathbf{n} p_F dS = \int_{\partial\Omega_{FS}} \mathbf{N}_S^T \mathbf{n} \mathbf{N}_F dS \mathbf{p}_F \tag{2.30}$$

From equation 2.26 the $\mathbf{f}_c$ for the acoustic domain is coupled using equation 2.18 and equation 2.27. Then $\mathbf{f}_c$ is formulated with relation to the structural acceleration.

$$\mathbf{f}_c = -c_0^2 \int_{\partial\Omega_{FS}} \mathbf{N}_F^T \mathbf{n}^T \nabla p_F dS = -\rho_0 c_0^2 \int_{\partial\Omega_{FS}} \mathbf{N}_F^T \mathbf{n}^T \mathbf{N}_S dS \ddot{\mathbf{d}}_\mathbf{S} \tag{2.31}$$

A spatial coupling matrix is defined and presented in equation 2.32.

$$\mathbf{H}_{FS} = \int_{\partial\Omega_{FS}} \mathbf{N}_S^T \mathbf{n} \mathbf{N}_F dS \tag{2.32}$$

Then the $\mathbf{f}_a$ force for the structural domain and the $\mathbf{f}_c$ for the acoustic domain can be expressed as the coupling forces in equation 2.33.

$$\mathbf{f}_a = \mathbf{H}_{SF}\mathbf{p}_F \qquad \mathbf{f}_c = -\rho_0 c_0^2 \mathbf{H}_{SF}^T \ddot{\mathbf{d}}_S \tag{2.33}$$

Finally, the two way system coupling matrix is expressed in equation 2.34 for an unsymmetrical system. And generalized in equation 2.35.

$$\begin{bmatrix} \mathbf{M}_S & 0 \\ \rho_0 c_0^2 \mathbf{H}_{SF}^T & \mathbf{M}_F \end{bmatrix} \begin{bmatrix} \ddot{\mathbf{d}}_\mathbf{S} \\ \ddot{\mathbf{p}}_\mathbf{F} \end{bmatrix} + \begin{bmatrix} \mathbf{K}_S & -\mathbf{H}_{SF} \\ 0 & \mathbf{K}_F \end{bmatrix} \begin{bmatrix} \mathbf{d}_S \\ \mathbf{p}_F \end{bmatrix} = \begin{bmatrix} \mathbf{f}_b \\ \mathbf{f}_q \end{bmatrix} \tag{2.34}$$

$$\mathbf{M}_{TOT}\ddot{\mathbf{U}} + \mathbf{K}_{TOT}\mathbf{U} = \mathbf{F}_{TOT} \tag{2.35}$$

2.1.5 Damped coupled system

If any material damping is applied or other acoustic energy dissipated, it is necessary to introduce a damping matrix to the dynamics [14]. The FE formulation for the derivations including damping are approximately the same as in the previous sections, and well described by, Zienkiewics [10] and PLM Software [15].

The general dynamic equations for a damped coupled system are expressed in equation 2.36. $\mathbf{F}_S^{TOT}$ and $\mathbf{F}_F^{TOT}$ are all loads for the structural and acoustic domain. An even more generalized system is expressed in equation 2.37.

$$\begin{bmatrix} \mathbf{M}_S & 0 \\ \mathbf{H}_{SF}^T & \mathbf{M}_F \end{bmatrix} \begin{bmatrix} \ddot{\mathbf{d}}_\mathbf{S} \\ \ddot{\mathbf{p}}_\mathbf{F} \end{bmatrix} + \begin{bmatrix} \mathbf{C}_S & 0 \\ 0 & \mathbf{C}_F \end{bmatrix} \begin{bmatrix} \dot{\mathbf{d}}_S \\ \dot{\mathbf{p}}_F \end{bmatrix} + \begin{bmatrix} \mathbf{K}_S & \mathbf{H}_{SF} \\ 0 & \mathbf{K}_F \end{bmatrix} \begin{bmatrix} \mathbf{d}_S \\ \mathbf{p}_F \end{bmatrix} = \begin{bmatrix} \mathbf{F}_S^{TOT} \\ \mathbf{F}_F^{TOT} \end{bmatrix} \tag{2.36}$$

$$\mathbf{M}^{TOT}\ddot{\mathbf{U}} + \mathbf{C}^{TOT}\dot{\mathbf{U}} + \mathbf{K}^{TOT}\mathbf{U} = \mathbf{F}^{TOT} \tag{2.37}$$

2.2 Eulerian-Lagrangian theory

In an Eulerian-Lagrangian analysis the materials involved is treated with two very different theories. The Eulerian material can be said to flow through the elements. The nodes are fixed in space, so that the elements are also fixed in space, but within an Eulerian element the volume fraction of material is not constant, as in the Lagrangian theory. This means that a single element have a material volume fraction ranging from 0 to 1, called Eulerian volume fraction (EVF) [9]. Previous work from Benson [6, 7] and Bathe [8] are considered through the following sections, among work from Belytschko [16],Hughes [17],Donèa [18] and Sahu [19]. Coupled Eulerian-Lagrangian (CEL) are a method developed to take benefit from the strengths in each method. The advantage is that the Eulerian mesh nodes always stays fixed so there will be no distortion of the mesh. This is a big advantage in case of large distortions. The property of the Eulerian formulation, and the EVF, i.e that the elements can possess a material volume fraction, induces difficulties at the contact regions of the different domains. A loss of accuracy, issues tracking free surfaces as the nodes does not coincide, and problems that the Eulerian material is penetrating through the Lagrangian [9]. However the CEL technique is a branch of the arbitrary Lagrangian-Eulerian (ALE) which offers more sophisticated methods to model complex problems. In some cases it might be necessary to allow a moving mesh together with the moving fluid. Even heat variation and compressibility might be evaluated in advanced systems. The complete explanation for such system will be described in the following sections. Figure 2.1 from Benson [7], illustrates the Lagrangian and Eulerian properties.
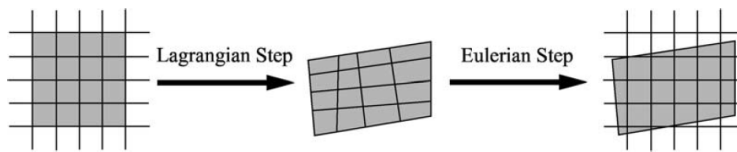

Figure 2.1: Lagrangian and Eulerian formulation.

2.2.1 Governing equations

The equation 2.38 for the structure are now presented where $\boldsymbol{\sigma}_S$ is the stress tensor, $\mathbf{b}_S$ is the body forces, ρ_S is the structural density and $\mathbf{u}_S$ is the displacement.

$$
\begin{cases}
\rho_S \frac{\partial^2 \mathbf{u}_S}{\partial t^2} = \tilde{\nabla}^T \cdot \boldsymbol{\sigma}_S + \mathbf{b}_S & \Omega_S \\
+B.C
\end{cases}
\tag{2.38}
$$

The fluid is described trough the Navier-Stokes equations which is also called Euler equations when thermal conductivity and viscosity is zero.

Equations 2.39a, 2.39b, 2.39c are the momentum equation, conservation of mass equation and conservation of energy equation. The notations are as follows, $\boldsymbol{\sigma}_F$ is the fluid stress tensor, $\mathbf{b}_F$ is the body forces for the fluid, ρ_F is the fluid density and $\mathbf{v}_F$ is the velocity of the fluid.

The previously discussed need for an analysis with moving mesh or thermal properties are described with notation, $\tilde{\mathbf{v}}$ for the mesh velocity for the moving arbitrary Lagrangian-Eulerian frame, $\mathbf{g}_F$ is the heat flux vector and g_F is the rate of heat per unit volume. Also $\mathbf{D}_F$ is the velocity strain tensor and e is the specific internal energy.

For a fluid problem assumed to be incompressible, inviscid and not with a moving mesh, the momentum equation 2.39a can be solved for $\tilde{\mathbf{v}} = 0$ and equation 2.39b for the conservation of mass reduces to $\nabla \cdot \mathbf{v}_F = 0$. The energy equation 2.39c then becomes excessive.

However, in the simulation the fluid is dedicated with a viscosity but a moving mesh is not considered.

$$
\begin{cases}
\begin{cases}
\rho_F \frac{\partial \mathbf{v}_F}{\partial t} + \rho_F [(\mathbf{v_F} - \tilde{\mathbf{v}}) \cdot \nabla] \mathbf{v}_F = \nabla \cdot \boldsymbol{\sigma}_F + \mathbf{b}_F & ,\Omega_F \\
+BC
\end{cases} & \text{(2.39a)} \\[2em]
\begin{cases}
\frac{\partial \rho_F}{\partial t} + (\mathbf{v_F} - \tilde{\mathbf{v}}) \cdot \nabla \rho_F + \rho_F \nabla \cdot \mathbf{v}_F = 0 & ,\Omega_F \\
+BC
\end{cases} & \text{(2.39b)} \\[2em]
\begin{cases}
\rho_F \frac{\partial e}{\partial t} + \rho(\mathbf{v_F} - \tilde{\mathbf{v}}) \cdot \nabla e = \boldsymbol{\sigma}_F \cdot \mathbf{D}_F - \nabla \cdot \mathbf{g}_F + g_F & ,\Omega_F \\
+BC
\end{cases} & \text{(2.39c)}
\end{cases}
$$

To ensure compatibility at the boundaries, the coupling equations 2.40 must be satisfied. Notations are as follows, $\mathbf{u}_S$ is the displacement of the structure, $\dot{\mathbf{u}}_S$ is the velocity of the structure and $\ddot{\mathbf{u}}_S$ is the acceleration of the structure. $\mathbf{u}_F$ is the displacement of the fluid, $\dot{\mathbf{u}}_F = \mathbf{v}_F$ is the velocity of the fluid and $\ddot{\mathbf{u}}_F = \dot{\mathbf{v}}_F$ is the acceleration of the fluid. $\boldsymbol{\sigma}_S$ and $\boldsymbol{\sigma}_F$ are the stress tensors of the structure and fluid. $\mathbf{n}$ is a unit normal vector.

$$
\begin{cases}
\boldsymbol{\sigma}_S \cdot \boldsymbol{n} = \boldsymbol{\sigma}_F \cdot \boldsymbol{n} & \Omega_{FS} \\[2mm]
\mathbf{u}_S = \mathbf{u}_F & \Omega_{FS} \\[2mm]
\dot{\mathbf{u}}_S = \dot{\mathbf{u}}_F = \mathbf{v}_F & \Omega_{FS} \\[2mm]
\ddot{\mathbf{u}}_S = \ddot{\mathbf{u}}_F = \dot{\mathbf{v}}_F & \Omega_{FS}
\end{cases}
\tag{2.40}
$$

2.2.2 FE formulation for structural domain

The derivation for the solid structure will be the same as described in chapter 2.1.2, where $\mathbf{f}_b$ is external forces and $\mathbf{f}_a$ are known linearizations.

$$
\mathbf{M}_S \ddot{\mathbf{u}}_S + \mathbf{K}_S \mathbf{u}_S = \mathbf{f}_b - \mathbf{f}_a
\tag{2.41}
$$

2.2.3 FE formulation for Eulerian domain

The constitutive equation for the fluid is expressed in equation 2.42 where $\mathbf{I}$ is the identity tensor, p_F is the fluid pressure and η and κ are the first and second coefficients for the viscosity. The velocity strain tensor $2\mathbf{D}_F = \nabla \mathbf{v}_F + (\nabla \mathbf{v}_F^T)$

$$
\boldsymbol{\sigma}_F = [-p_F + \eta \nabla \cdot \mathbf{v}_F]\mathbf{I} + 2\kappa \mathbf{D}_F
\tag{2.42}
$$

The relation between the viscosity coefficients are.

$$
\eta = -\frac{2}{3}\kappa
\tag{2.43}
$$

For application with heat transfer the constitutive relation is shown in equation 2.44, where $\mathbf{g}_F$ is the heat transfer, T is the temperature and $\mathbf{k}$ is the conductivity tensor.

$$\mathbf{g}_F = -\mathbf{k}\nabla T \tag{2.44}$$

The density ρ_F and energy e also becomes a function of both pressure and temperature so the relations in equation 2.45 needs to be taken into account when solving 2.39a, 2.39b and 2.39c.

$$\begin{aligned} \rho_F &= \rho_F(p_F, T) \\ e &= e(p_F, T) \end{aligned} \tag{2.45}$$

For the case of an operating Francis turbine or just a general fluid-fluid interface it might be favorable to simulate with a moving mesh at the boundaries. A displacement $\tilde{\mathbf{u}}$ would then represent the moving mesh at the boundary Ω_{FS}. The unit normal vector $\mathbf{n}$ and unit tangential vector $\mathbf{t}$ are used to describe the motion of the mesh in the desired directions. The expression of the displacements can then be expressed in $\tilde{u}_n$ and $\tilde{u}_t$.

$$\begin{aligned} \tilde{\mathbf{u}} \cdot \mathbf{n} &= \tilde{u}_n \quad \Omega_{Fs} \\ \tilde{\mathbf{u}} \cdot \mathbf{t} &= \tilde{u}_t \quad \Omega_{FS} \end{aligned} \tag{2.46}$$

The finite element equations for the fluid with assumed moving mesh is then described in equation 2.47, where $\tilde{\mathbf{v}}$ and $\tilde{\mathbf{u}}$ are the velocity and displacement vectors of the moving mesh. Note that these vectors may be overlapping and contain vectors of different units.
$\dot{\mathbf{v}}_F$ and $\mathbf{v}_F$ are the fluid acceleration and velocity vectors. $\tilde{\mathbf{M}}$ and $\tilde{\mathbf{K}}$ are the tangent mass and stiffness matrix for the arbitrary Lagrangian-Eulerian that couples the acceleration and displacement of the mesh. $\mathbf{f}_q$ are the external forces and $\mathbf{f}_c$ are known.

$$\begin{bmatrix} \mathbf{M}_F & \tilde{\mathbf{M}} \end{bmatrix} \begin{bmatrix} \dot{\mathbf{v}}_F \\ \tilde{\mathbf{v}} \end{bmatrix} + \begin{bmatrix} \mathbf{K}_F & \tilde{\mathbf{K}} \end{bmatrix} \begin{bmatrix} \mathbf{v}_F \\ \tilde{\mathbf{u}} \end{bmatrix} = \mathbf{f}_q - \mathbf{f}_c \tag{2.47}$$

2.2.4 FE formulation for the coupled system

The coupled system of equations can again be described by the general dynamic equation for a coupled system, shown in equation 2.48. $\mathbf{R}$ are all forces in the system. The $\mathbf{T}_2$ matrix containing both masses and stiffness due to the moving mesh. Therefore the displacement vector $\mathbf{U}$ also contains new vectors representing displacement, velocities or both in $\mathbf{u}_{FS}$. The complexity beyond this simple generalization is crude, and comes as a result of the implementation of the moving mesh.

$$\mathbf{T}_1\ddot{\mathbf{U}} + \mathbf{T}_2\dot{\mathbf{U}} + \mathbf{T}_3\mathbf{U} = \mathbf{R} \tag{2.48}$$

Equation 2.49 shows how the $\mathbf{U}$ vector can be represented and contains new vectors.

$$\mathbf{U} = \begin{bmatrix} \mathbf{u}_S \\ \mathbf{u}_{FS} \\ \mathbf{u}_F \end{bmatrix} \tag{2.49}$$

2.2.5 Damped coupled system

For additional damping applied to the system a $\mathbf{T}_4$ matrix is added to represent the damping at any of the domains, i.e the whole system. This is more comprehensible than implementing the additional damping into the already complex $\mathbf{T}_2$ matrix .

$$\mathbf{T}_1\ddot{\mathbf{U}} + (\mathbf{T}_2 + \mathbf{T}_4)\dot{\mathbf{U}} + \mathbf{T}_3\mathbf{U} = \mathbf{R} \tag{2.50}$$

2.3 Logarithmic decrement and damping ratio

The logarithmic decrement δ definition in equation 2.51 are defined as the natural log of the ratio between two amplitude peaks [20, 21]. Figure 2.2 illustrates such amplitude peaks. In the case where the the peaks are next to each other $n = 1$, but the argument is valid for any amplitude peak $n = N$. The logarithmic decrement is an experimental way for determination of the damping ratio ζ, equation 2.52 shows the damping ratio equation.

$$\delta = \frac{1}{n} \ln \left| \frac{x(t)}{x(t + nT)} \right| \tag{2.51}$$

$$\zeta = \frac{1}{\sqrt{1 + (\frac{2\pi}{\delta})^2}} \tag{2.52}$$

Figure 2.2 illustrates a system with damped oscillations. A system with a damping ratio, $\zeta < 1$ is an underdamped system. Assuming that equation 2.53 is the characteristic equation of motion for the underdamped system. This enables us to express the response of the oscillating system at any time. Equation 2.54 describes one period of the oscillations , i.e from one peak to the next peak.
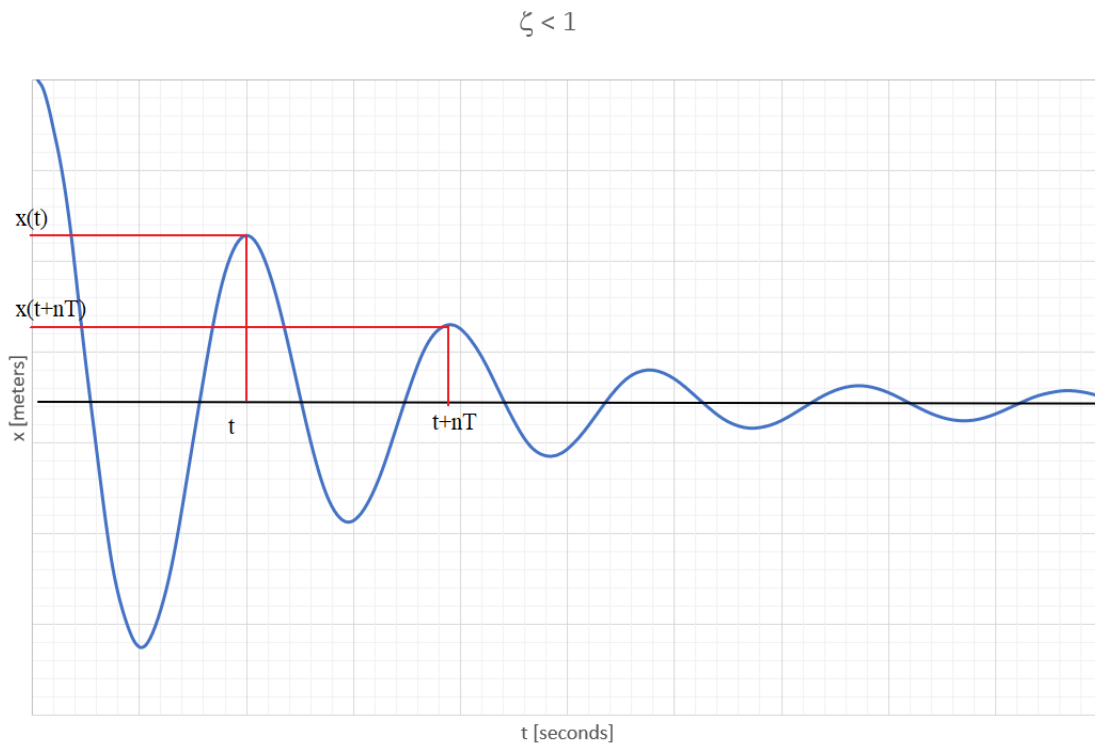

Figure 2.2: Logarithmic decrement determination from response graph.

$$x(t) = A\exp^{(-\zeta\omega_n t)}\sin{(\omega_d t + \phi)} \tag{2.53}$$

$$T = \frac{2\pi}{\omega_d} \tag{2.54}$$

Using the definition for the logarithmic decrement and plug in the characteristic motion equation with correct time for each amplitude peak, a proof for the validation of equation 2.52 will be derived. Keep in mind the relation expressed in equation 2.55, and the definition for the damping frequency ω_d of an underdamped system in equation 2.56.

$$\sin[\omega_d(t + nT) + \phi] \stackrel{2.54}{=} \sin(\omega_d t + 2\pi n + \phi) = \sin(\omega_d t + \phi) \tag{2.55}$$

$$\omega_d = \omega_n\sqrt{(1 - \zeta^2)} \tag{2.56}$$

$$\delta = \ln\left[\frac{x(t)}{x(t+nT)}\right] = \ln\left[\frac{A\exp^{(-\zeta\omega_n t)}\sin(\omega_d t + \phi)}{A\exp^{-\zeta\omega_n(t+nT)}\sin[\omega_d(t+nT)+\phi]}\right]$$

$$= \ln\left[\frac{A\exp^{(-\zeta\omega_n t)}\sin(\omega_d t + \phi)}{A\exp^{-\zeta\omega_n t}\cdot\exp^{-\zeta\omega_n nT}\sin[\omega_d(t+nT)+\phi]}\right]$$

$$= \ln\left[\frac{\sin(\omega_d t + \phi)}{\exp^{-\zeta\omega_n nT}\sin[\omega_d(t+nT)+\phi]}\right]$$

$$= \ln\left[\frac{\sin(\omega_d t + \phi)}{\exp^{-\zeta\omega_n nT}\sin(\omega_d t + \omega_d nT + \phi)}\right]$$

$$= \ln\left[\frac{\sin(\omega_d t + \phi)}{\exp^{-\zeta\omega_n nT}\sin(\omega_d t + 2\pi n + \phi)}\right]$$

$$= \ln\left[\frac{1}{\exp^{-\zeta\omega_n nT}}\right]$$

$$= \zeta\omega_n nT \tag{2.57}$$

$$= \frac{\zeta\omega_n n2\pi}{\omega_d}$$

$$= \frac{\zeta\omega_n n2\pi}{\omega_n\sqrt{(1-\zeta^2)}}$$

$$= \frac{\zeta n2\pi}{\sqrt{(1-\zeta^2)}}$$

$$\overset{n=1}{=} \frac{\zeta 2\pi}{\sqrt{(1-\zeta^2)}}$$

$$\Rightarrow \zeta = \frac{1}{\underline{\underline{\sqrt{1 + (\frac{2\pi}{\delta})^2}}}} \qquad q.e.d$$

After some algebra the damping ratio ζ can finally be expressed as previous presented in equation 2.52.

2.4 Abaqus units

Abaqus has no built-in unit system, which presupposes that the user keeps track of all units [22]. This imposes the user to be extra careful defining the parameters used in the models, setup of the analysis and interpretation of the results.

Through this master thesis, **SI(mm)** units are used. The choice of **SI(mm)**) units are mainly due to convenience when dealing with small scale models.

Consistent units				
Quantity	SI	SI (mm)	US Unit (ft)	US Unit (inch)
Length	m	mm	ft	in
Force	N	N	lbf	lbf
Mass	kg	tonne (10^3 kg)	slug	lbf s^2/in
Time	s	s	s	s
Stress	Pa (N/m^2)	MPa (N/mm^2)	lbf/ft^2	psi (lbf/in^2)
Energy	J (N × m)	mJ (10^{-3} J)	ft lbf	in lbf
Density	kg/m^3	tonne/mm^3	slug/ft^3	lbf s^2/in^4

Figure 2.3: Abaqus unit system.

2.5 Energy

To evaluate the validity of the model setup and results from an Abaqus explicit analysis, the concept of energy balance can be utilized. This gives the user insight whether the simulation is responding sufficiently within the demands, or is diverging [23]. If the numerical analysis are "leaking energy", it indicates that it may be something wrong with the analysis setup or an even more complicated issue with the model. This section will introduce a simplified version of the energy concept, and for the interesting reader the integral forms of the energy equations can be found in the Abaqus theory [24].

The total energy, ETOTAL should be constant for an ideal system. It is important to underline that the total energy should not be necessarily zero in a dynamic analysis, but constant. In a finite element analysis, the total energy may vary due to many reasons, such as the numerical

approximations in the finite element algorithms and meshing, non-linearity, hour glassing or energies not taken into account in the model.

"The sum of these energy components is E_{total} , which should be constant. In the numerical model E_{total} is only approximately constant, generally with an error of less than 1%"[25].

Equation 2.58 is the energy balance equation for the CAS analysis and CEL analysis. For other types of numerical analysis a more complementary set of energy variables may be taken into account, if the case of contact penalties, heat, friction forces or other parameters. It is up to the user to decide the importance of the parameters and their associated energies. The total energy balance is only available for the whole model in Abaqus explicit.

$$ETOTAL = ALLIE + ALLVD + ALLFD + ALLKE - ALLWK = CONSTANT \tag{2.58}$$

- ETOTAL is the total energy
- ALLIE is the internal energy
- ALLVD is the energy absorbed by viscous dissipation
- ALLFD is the frictional dissipation energy
- ALLKE is the kinetic energy
- ALLWK is the work of external forces

3 Numerical methods

The differences of the CAS and the CEL simulations are significant, and the trade-off between advantages and disadvantages from one method to the other, becomes very clear when applied to the same problem. The domains representing the surrounding water, i.e the acoustic domain and Eulerian domain have different features and behaviour, especially from a simulation point of view. For example the acoustic elements are not applicable with a gravity load, while the Eulerian elements offer this choice. For the acoustic elements the gravity load must be represented with an impedance, which can be challenging. In order to have two comparable simulations the gravity load is therefore left out from both analysis, as the gravity load is left out from the simulations so its potential damping effect from gravity. A broad variety of parameters need to be considered trying to unify the complex nature of the problems. The immersed structure and the surrounding fluid are therefore subjected with different assumptions trying to unify them as equal simulations. This is described through the following sections and in detail described in appendix A and appendix C. Both simulation are executed with Abaqus dynamic explicit [26], which eliminates the problem for the user to define the time step increments.
The explicit solver calculates the stable time increments for the analysis.

3.1 Acoustic-structure method

3.1.1 Material properties and dimensions

Material properties and dimensions for the structural domain and acoustic domain are tabulated in table 3.1 and table 3.2. In the structural domain ρ_S, is the density, E is the elastic modulus and v is the Poisson ratio. For the acoustic domain, ρ_F is the density and K_F is the bulk modulus.

$Parameter$	$\rho_S \left[\frac{ton}{mm^3} \right]$	$E \left[\frac{N}{mm^2} \right]$	$v \left[- \right]$	$L \left[mm \right]$	$W \left[mm \right]$	$H \left[mm \right]$
$Value$	$7850e^{-12}$	$200e^3$	0.3	200	20	5

Table 3.1: Properties and dimensions of structural domain.

22

$Parameter$	$\rho_F \left[\frac{ton}{mm^3}\right]$	$K_F \left[\frac{N}{mm^2}\right]$	$L \left[mm\right]$	$W \left[mm\right]$	$H \left[mm\right]$
$Value$	$1000e^{-12}$	2200	400	60	400

Table 3.2: Properties and dimensions of acoustic domain.

3.1.2 Mesh

To ensure coincide nodes at the boundary of the domains, both meshes are of structured hexahedron type. This avoids difficulties connecting the elements associated with the domains and reduces the error and computation time due to automatic node adjustment. The structural mesh is of 2.5 mm in y-direction and 5 mm in the z-direction and x-direction, while the acoustic mesh is 2.5 mm in the y-direction and 10 mm in the z-direction and x-direction in the boundary region and surrounding region of importance. Elsewhere the global acoustic mesh size is 10 mm. Figure 3.1 illustrates that nodes will be perfect coincide in an assembly.

Structural elements are of type C3D8R and the acoustic elements are of type AC3D8R, this implies that both meshes offers reduced integration with hourglass control [27]. Hourglass control is a method controlling that the elements do not exceed a certain limit of deformation.
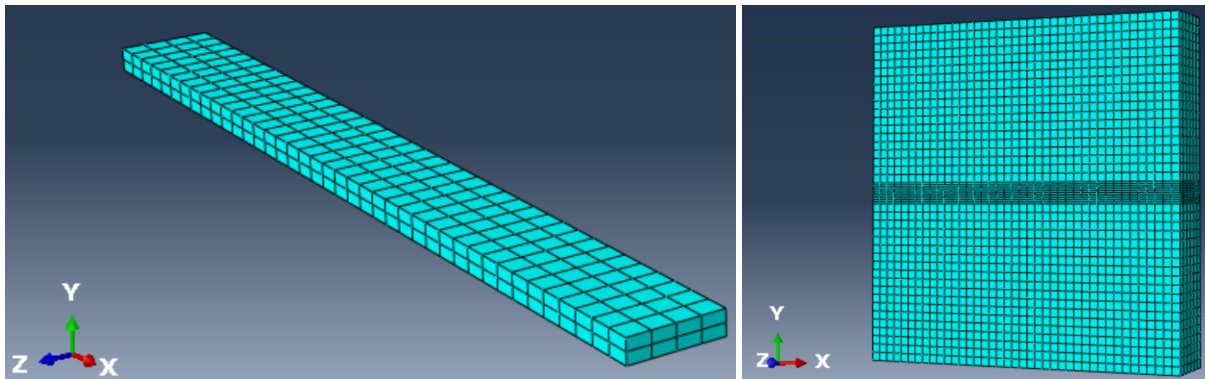

Figure 3.1: Structural and acoustic mesh

Domain	Number of elements
Structural	320
Acoustic	11440
Total	11760

Table 3.3: Mesh statistic CAS.

3.1.3 Interactions, boundary conditions and loads

In the acoustic domain all outer surface walls are assigned non-reflecting planar acoustic impedance. This assumption gives that the acoustic waves will not reflect back and forth in the model and eliminate the vibrations caused by reflection of the acoustic waves. For a real situation this will replicate that the structure is immersed in a almost infinite big fluid container.

The structure is fixed in all directions at one end and free to oscillate at the other. Connecting the structural mesh to the acoustic mesh is done by using tie constraints at the boundary, also the feature acoustic interface will then be automatic set to the regions where the tie constrains are applied. All connected nodes are within the default position tolerances of the software.

An instantaneous load of 10 N is applied in negative the y-direction, i.e at the xz-plane. The position is chosen to be centered and 10 mm from the tip of the structure. This completes the setup of boundary conditions, interactions and loads of the acoustic-structure numerical analysis. A detailed explanation of the complete model setup can be found in appendix A.
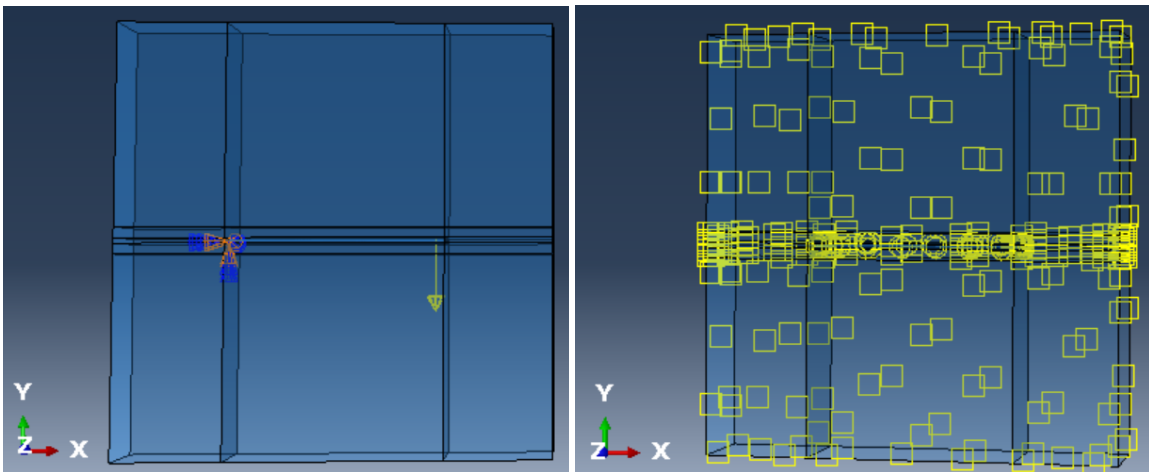

Figure 3.2: Transparent view of load, boundary conditions and interactions.

3.1.4 Step and job

The total duration for the analysis is 0.2 seconds and non-linear geometry of toggled on. The default option of automatic incrementation is chosen, and the stable time increment is calculated to be $3.68479e - 07s$ for the analysis.

In the job module the choice of using multiple processors are toggled on, the computer have four available and all are chosen. In addition the Abaqus explicit precision is set to double for analysis only. This is to reduce accumulation of numerical errors in the case of a large number of total increments, which for the analysis are 542773 increments.

3.2 Eulerian-Lagrangian method

3.2.1 Material properties and dimensions

The structural parameters and dimensions are constant throughout both analysis and therefore exactly the same as described in table 3.1.
Parameters for the Eulerian domain are shown in table 3.4, where ρ_F is the density, κ is the dynamic viscosity and c_1 is the speed of sound in the fluid. Using the Eulerian formulation gives the opportunity to follow the fluid flow passing through the fixed Eulerian mesh. To fill and assign the qualities of an Eulerian fluid to a domain, the volume fraction tool must be utilized [28]. Together with the feature, predefined field, this gives a complete material assignment.
The Eulerian volume fraction (EVF) tool now enables an element to be fully, partially or empty of a material. An element completely empty of material is just filled with void and possesses no integrity.

$Parameter$	$\rho_F \left[\frac{ton}{mm^3}\right]$	$c_1 \left[\frac{mm}{s}\right]$	$\kappa \left[\frac{Ns}{mm^2}\right]$	$L \left[mm\right]$	$W \left[mm\right]$	$H \left[mm\right]$
$Value$	$1000e^{-12}$	$1.5e^6$	$1e^{-9}$	400	60	400

Table 3.4: Properties and dimensions of Eulerian domain.

3.2.2 Mesh

Producing the mesh for the CEL analysis is done under the same prerequisites as for the CAS analysis to obtain consistency between the two methods. The volume fraction tool needed to be used for filling purposes of the Eulerian properties into the region, requires a dummy container to be designed and meshed. This is a discrete rigid container, meshed with R3D4 mesh. This part is suppressed during the simulation and therefore not accounted for in total numbers of elements in table 3.5.

The Eulerian region are assigned EC3D8R mesh and are only available in Abaqus explicit. This mesh are as mentioned fixed in space, but allows the fluid to flow freely between the elements due to the advanced volume fraction tool.

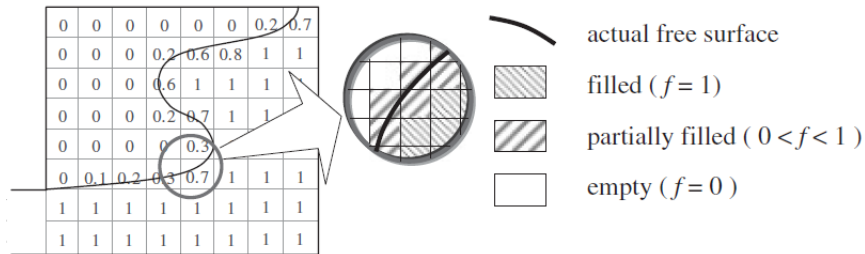Figure 3.3 illustrates the volume fraction principle in the fixed Eulerian mesh [29].

Figure 3.3: Fixed grid with containing VOF.

The structural mesh are consistent and same in both analysis, and of element type C3D8R. From figure 3.4 it can be observed that the Eulerian mesh and the dummy mesh, are both dedicated the dimensions given above in table 3.4. Due to the suppression of the dummy mesh these elements are not taken into consideration for the total number of elements in the analysis, given in table 3.5.
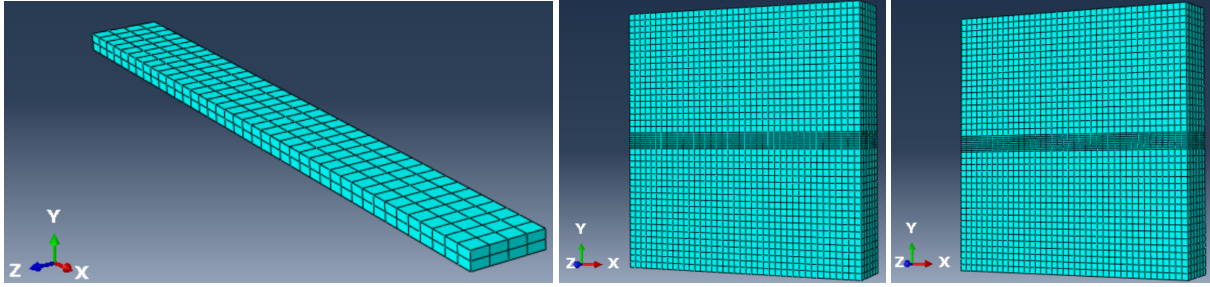
Figure 3.4: Structural,Eulerian and dummy mesh

Domain	Number of elements
Structural	320
Eulerian	11520
Dummy*	5064
Total	11840
*Suppressed,just for filling purpose.	

Table 3.5: Mesh statistic CEL.

3.2.3 Interactions, boundary conditions and loads

Interaction properties between the structural and Eulerian domain are specified to general contact. The assumptions are frictionless tangential behavior and hard contact in normal direction. The need for using the general contact interaction in this analyse are due to the properties of the Eulerian behavior. Node to node contact are therefore impossible.

For the Eulerian domain the outer walls are assigned with free inflow and non-reflecting outflow assumption. This boundary condition also eliminates vibrations caused by reflecting waves inside the domain and keep the fluid volume constant. The structure is fixed at one end with the encastre condition, and free to oscillate at the other.

An instantaneous load of 10 N is applied in negative y-direction, i.e at the xz-plane. The position is chosen to be centered and 10 mm from the tip of the structure. The Eulerian representation together with the EVF tool gives the opportunity to visually follow the fluid flow passing through the fixed mesh in the whole Eulerian domain. A detailed explanation of the complete model setup can be found in appendix C.
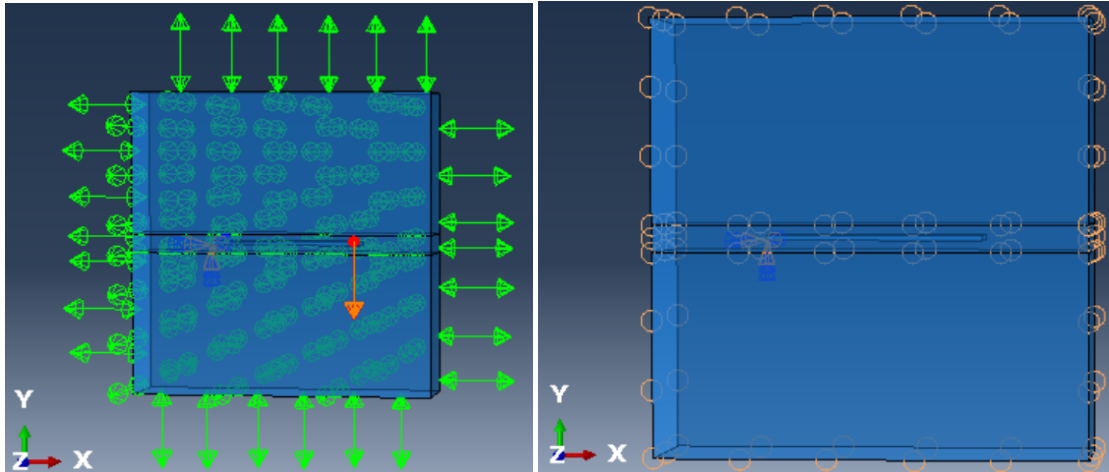
27

Figure 3.5: Transparent view of load, boundary conditions and interactions.

3.2.4 Step and job

The total duration for the analysis is 0.2 seconds and non-linear geometry are toggled on. The default option of automatic incrementation is chosen and stable time increment is calculated to be $3.1298e-07s$ for the analysis.

In the job module the choice of using multiple processors are also toggled on, the computer have four available and all are chosen. In addition, the Abaqus explicit precision is set to double for the analysis only. This is to reduce accumulation of numerical errors in case of large number of total increments. The total number of increments in the analysis are 639019.

4 Results and discussion

4.1 Displacement and damping

For the CAS analysis a displacement versus time plot in figure 4.1 is provided with 500 evenly spaced data points during the total analysis time. The plotted displacements are requested to be at the node where the instantaneous force of 10 N is exerted. In figure 4.2 a plot with the exact same prerequisites are provided for the CEL analysis. Comparison plot is provided in figure 4.3.
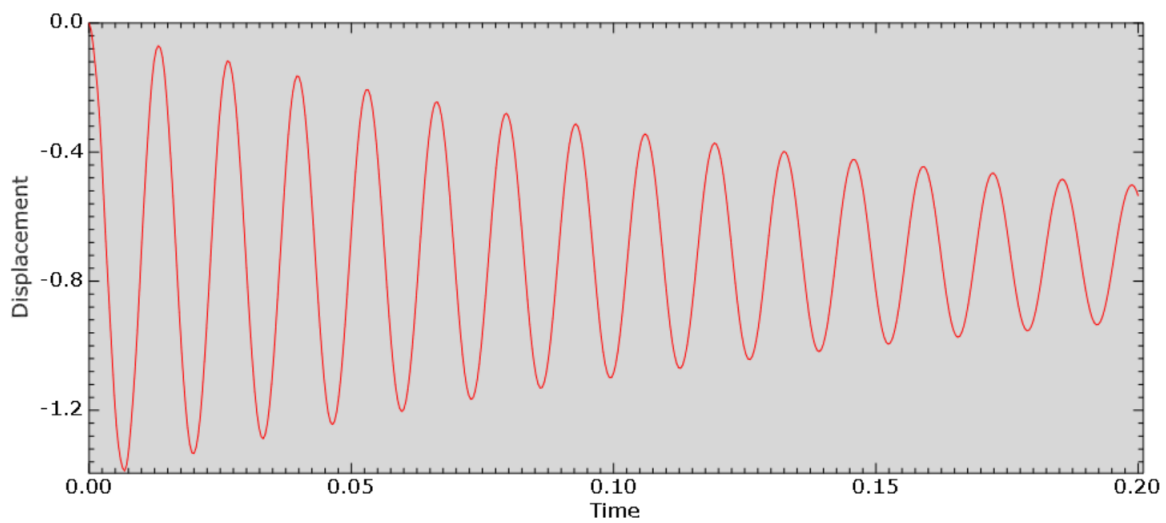

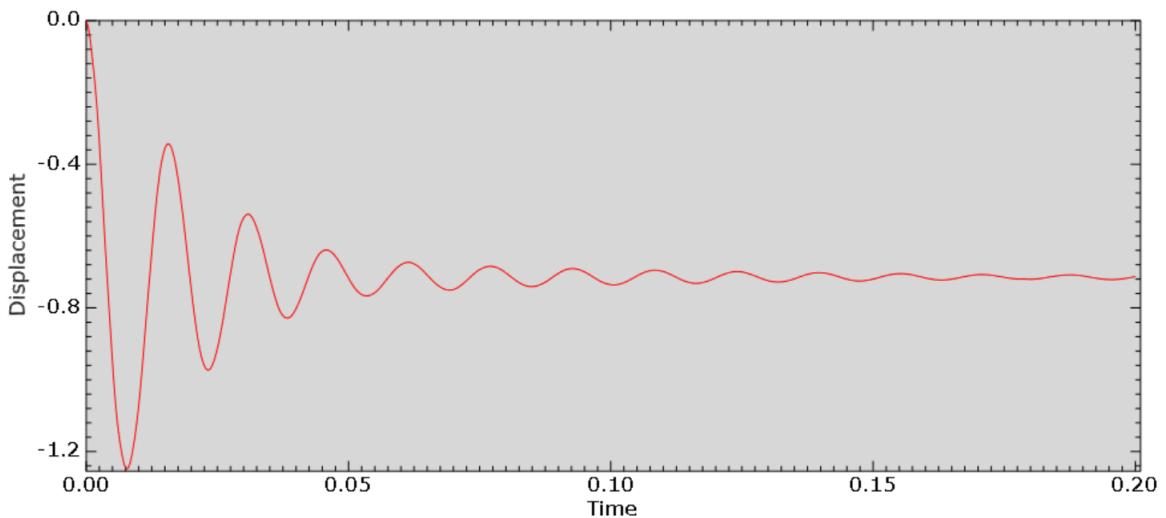Figure 4.1: Displacement at the force node CAS analysis.

Figure 4.2: Displacement at the force node CEL analysis.

By visualizing the results from the CAS analysis and CEL analysis in the same plot, the differences become clear. The decay rates of the amplitudes are of significant differences.

Reintroducing the logarithmic decrement equation 2.51, a measurement for the decaying harmonic oscillations are provided. Also reintroducing the equation for the damping ratio, earlier presented in equation 2.52, the tools for a mathematical evaluation of the harmonic oscillations are now in possession. Due to the numerical errors in the analysis there is a slight difference in the equilibrium lines, assuming that the average equilibrium line for both graphs are the same and equal $-0.710mm$. Note that the line for equilibrium are at this displacement because the instantaneous force is not released. The amplitude peaks from $[0:0.1]$ seconds are chosen for calculation of the logarithmic decrement and damping ratio for both analysis. The interval is mainly chosen because of the rapid decay in the CEL analysis, and it is therefore difficult to measure exact values out of this range.

Figure 4.3: Comparison of displacement at the force nodes.

$$\delta_{CAS} = \frac{1}{7} \ln \left| \frac{-0.710 - (-0.077)}{-0.710 - (-0.321)} \right| = \underline{\underline{0.070}} \qquad \zeta_{CAS} = \frac{1}{\sqrt{1 + (\frac{2\pi}{0.070})^2}} = \underline{\underline{0.011}} \qquad (4.1)$$

$$\delta_{CEL} = \frac{1}{6} \ln \left| \frac{-0.710 - (-0.348)}{-0.710 - (-0.685)} \right| = \underline{\underline{0.445}} \qquad \zeta_{CEL} = \frac{1}{\sqrt{1 + (\frac{2\pi}{0.445})^2}} = \underline{\underline{0.071}} \qquad (4.2)$$

Parameter	CAS	CEL
Logarithmic decrement δ	$\delta_{CAS} = 0.070$	$\delta_{CEL} = 0.445$
Damping ratio ζ	$\zeta_{CAS} = 0.011$	$\zeta_{CEL} = 0.071$
Period T	$T_{CAS} = 0.0132s$	$T_{CEL} = 0.0156s$
Frequency f	$f_{CAS} = 75.75Hz$	$f_{CEL} = 64.10Hz$

Table 4.1: Schematic representation.

The schematic representation of the results in table 4.1 shows that the logarithmic decrement results are non homogeneous for the CAS and CEL analysis. This also give rise for unequal damping ratios. A damping ratio $\zeta_{CAS} = 1.1\%$ for the CAS analysis and a damping ratio $\zeta_{CEL} = 7.1\%$ for the CEL analysis. A lower damping ratio for the CAS analysis was expected due to the fact that no viscosity was applied to the acoustic elements.

In order to compare the CAS and CEL analysis at equal conditions, a dynamic explicit simulation where run for both. By default, the dynamic explicit analysis introduce a linear and quadratic bulk viscosity. See appendix B and appendix D for values of the parameters. The linear and quadratic bulk viscosity are by default included in the explicit analysis for several reasons, such as to distribute a point shock load over several elements to avoid collapse. The properties of these parameters will lead to damping in the system. Documentation for the linear and quadratic bulk viscosity can for the interested reader be found at Abaqus user guide [26].

For the CAS analysis the results for the damping ratio $\zeta_{CAS} = 1.1\%$, period $T_{CAS} = 0.0132s$ and frequency $f_{CAS} = 75.75Hz$ are assumed to be strictly a consequence of the added mass of the surrounding acoustic elements and a small fraction from the linear and quadratic bulk viscosity.

31

In the CEL analysis a viscosity is specified for the Eulerian elements and therefore the damping ratio results are plausible and more realistic. Difference in the period $T_{CEL} = 0.0156$ compared to the period for the CAS analysis are also explained by the viscosity dedicated to the Eulerian elements. The viscosity applied to the Eulerian elements decrease the displacement already at the first oscillation peak of the immersed structure compared to the structure immersed in the acoustic elements.

The differences between the periods in the simulations are not remarkable big, but the presence of viscosity is clearly present. The frequencies are directly related to the period with the relation $f = \frac{1}{T}$, so the frequency $f_{CEL} = 64.10 Hz$ are therefore lower than for the CAS analysis. The damping ratio $\zeta_{CEL} = 7.1\%$ are considerable higher than for the CAS analysis, so the effects of the viscosity becomes clearly visible. It is therefore assumed in the CEL analysis, that the damping ratio is a consequence of the added mass of the water, liner and quadratic bulk and the viscosity applied.

An eigenfrequency analysis is not performed to any of the models, so it is yet to know if the frequencies are critical in regards to resonance.

4.2 Velocities

For the CAS and CEL analysis velocity versus time plots are provided in figure 4.4 and figure 4.5. The plots are made of 500 evenly spaced data points during the total analysis time. The plotted velocities are requested to be at the node where the instantaneous force of 10 N is exerted. A comparison plot for the velocities are also provided in figure 4.6.
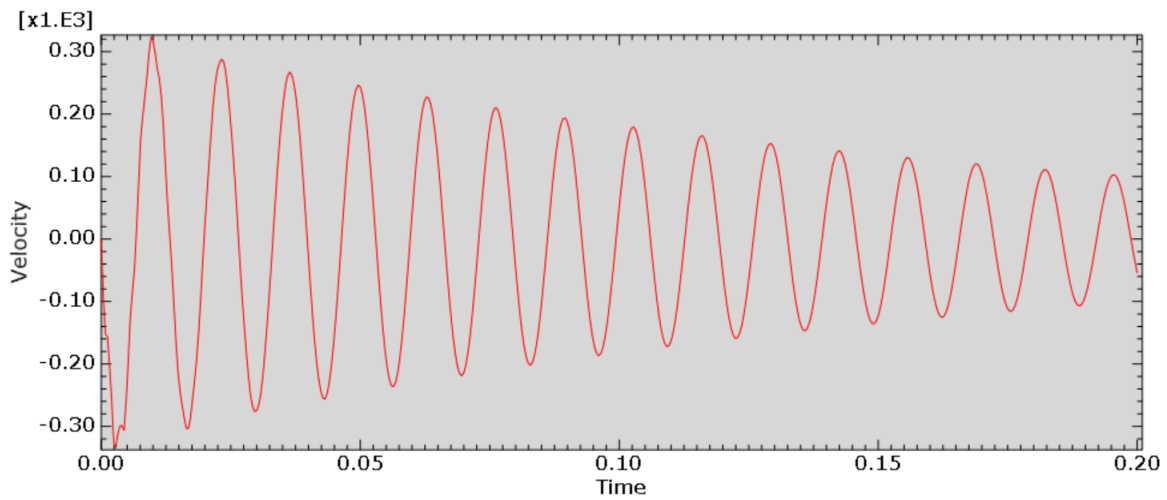

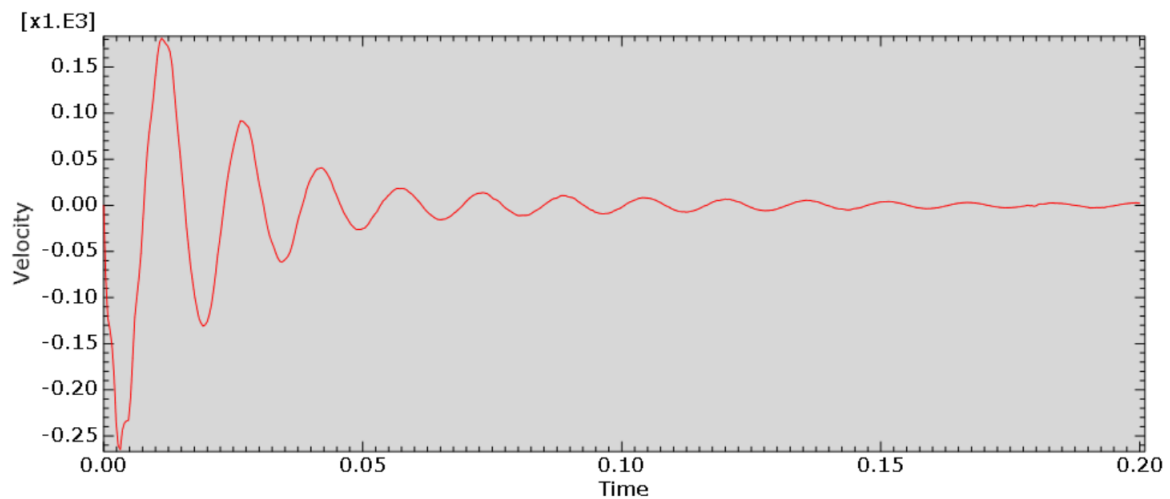Figure 4.4: Velocity at the force node CAS analysis.

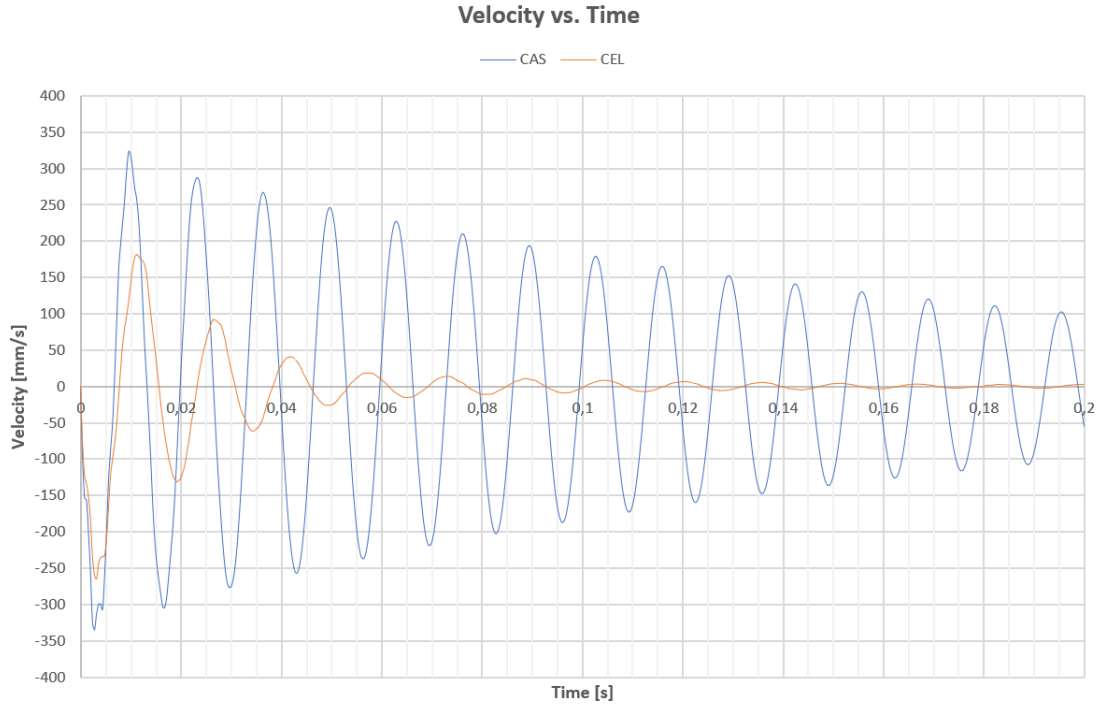Figure 4.5: Velocity at the force node CEL analysis.

Figure 4.6: Comparison of velocities.

The tendency for the velocities are the same as for the displacements and are also justified by the presence of viscosity added to the Eulerian elements in the CEL analysis. As previously not pointed out but worth noticing, is the strong influence the viscosity has in reduction of the first velocity amplitude peak. For an imagined case of surrounding structure containing critical components such as a valve or sensor, a pressure wave with the velocities plotted in the CEL analysis could have been within the limits, while a pressure wave with the velocities plotted for the CAS analysis could have been above. A similar analogy are also relevant or even more critical for the displacements, as that could have meant contact between structures.

This substantiate the importance of adding correct properties to achieve reliable results in dynamical simulations.

4.3 Kinetic energy

The kinetic energy for both models are plotted with 200 evenly spaced data points during the total analysis time. Figure 4.7 shows the kinetic energy for the CAS analysis and figure 4.8 shows the kinetic energy for the CEL analysis. In figure 4.9 a comparison of the kinetic energies are presented with associated polynomial trendlines of fifth degree. A polynomial line of this degree are exaggerated for the CAS analysis but a suitable fit for the CEL analysis.
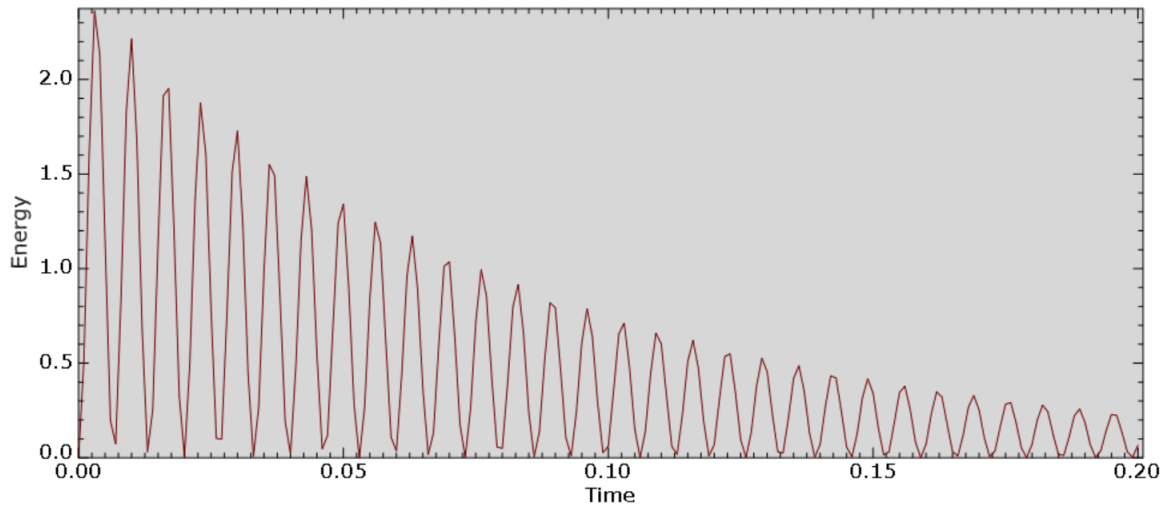

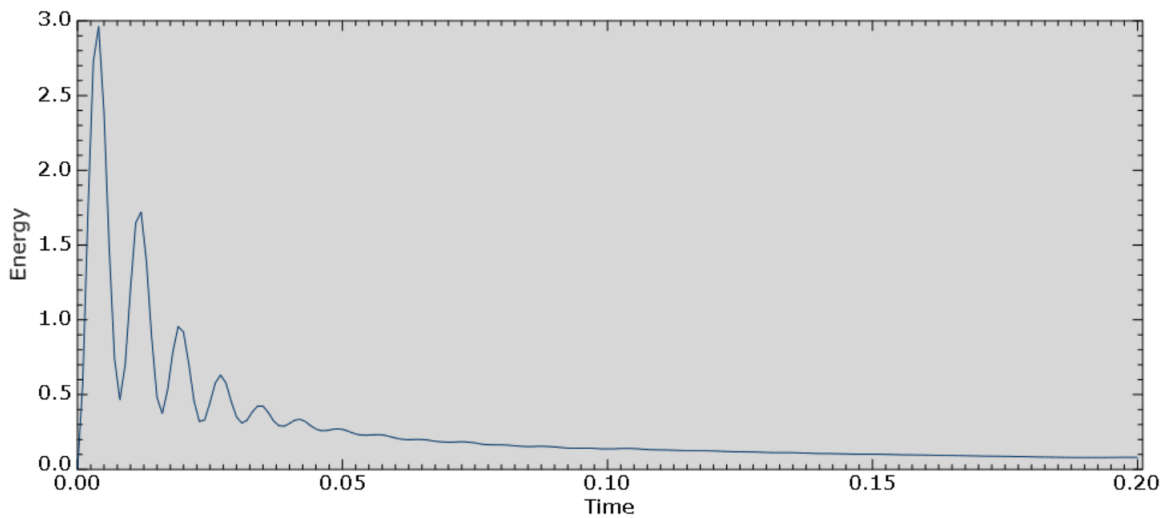Figure 4.7: Kinetic energy CAS model.

Figure 4.8: Kinetic energy CEL model.

Kinetic energy is the energy the system possesses due to its motion, also known as mechanical energy. The decrease of kinetic energy is clearly visible in both figures, meaning that the kinetic energy is converting into other types of energies. The conversion from kinetic energy into other types implies that less and less energy is left to oscillate the steel structure, so it is said to be damped.

For the CAS analysis a slow decay of kinetic energy can be observed, and the system still holds a substantial amount of kinetic energy at the end of the simulation period. The strong conservation of kinetic energy in the CAS analysis is due to the absence of acoustic impedance, damping or volumetric drag defined inside the model. Acoustic impedance is only defined at the outer surfaces of the model. For the record, acoustic impedance and volumetric drag in acoustic elements, can be thought of as the counterpart of damping mechanisms the viscosity causes in the Eulerian elements.

In the CEL analysis a rapid decay of kinetic energy is observed and an almost complete conversion of kinetic energy is registered at the end of simulation time $0.2s$. An assumption that the viscosity added to the Eulerian elements are the main reason to the rapid decay, implies that the kinetic energy is mainly converted into viscous dissipation energy. The viscous dissipation can be thought of as the damping mechanisms in the system, and the viscosity is therefore a large contributor to the damping.
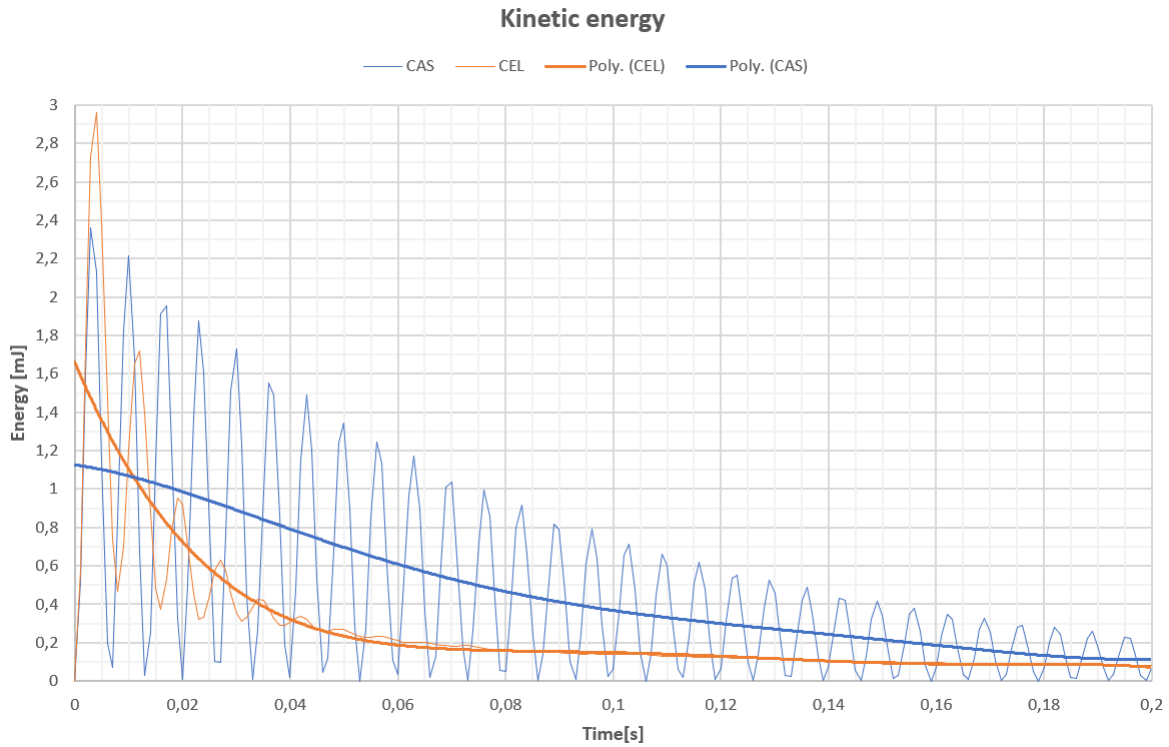
Figure 4.9: Comparison of kinetic energy.

The comparison figure 4.9 illustrates the large differences of the change of kinetic energy for both analysis. Both trendlines are approximated with a fifth degree polynomial as previously stated.

For the CAS analysis the trendline is almost linear, while for the CEL analysis the line could be described by an exponential function. The rapid decay of kinetic energy in the CEL analysis between $0s$ to $0.05s$ indicated that most of the conversation of kinetic energy into other energies are within this interval and almost constant after $0.05s$.

4.4 Viscous dissipation energy

The viscous dissipation for both models are plotted with 200 evenly spaced data points during the total analysis time. Figure 4.10 shows the viscous dissipation for the CAS analysis, and figure 4.11 shows the viscous dissipation for the CEL analysis. The viscous dissipation energy can be thought of as the mechanical energy the system convert into energy used for damping. The viscous dissipation energy is also irreversible, so the energy can not be converted back to mechanical energy. If there would be no viscous dissipation energy or other losses, the mechanical energy for the system would be conserved and fluctuate between kinetic and potential energy. The viscous dissipation energy includes the material damping, viscosity and bulk viscosity, and can in general be thought of as the damping mechanisms for the system. The reader is advised to note the scales of the vertical axes in the figures.

As no viscosity is defined for the acoustic elements, the viscous dissipation energy in the CAS analysis is quite small, and most likely induced by the previous discussed default values of linear and quadratic bulk viscosity which induces damping, or due to numerical errors. The applied acoustic impedance at the outer boundaries does also come into account. The expected dissipation for the CAS analysis are ideally equal to zero disregarded the default bulk viscosity parameter values and the boundary conditions. The total quantity of viscous dissipation energy for the CAS analysis are calculated to be $0.04994773 mJ$ during the simulation period of $0.2s$.

For the CEL analysis the values of the vertical axis are 1000 times greater than the values for the CAS analysis. This indicated that the Eulerian elements, with the added dynamic viscosity, have a strong ability to convert the mechanical energy into irreversible viscous dissipation energy. The high share of dissipation energy in the CEL analysis must therefore be the main contributor to the damping effects in the analysis. The total quantity of viscous dissipation energy for the CAS analysis are calculated to be $660.3630 mJ$ during the simulation period of $0.2s$.
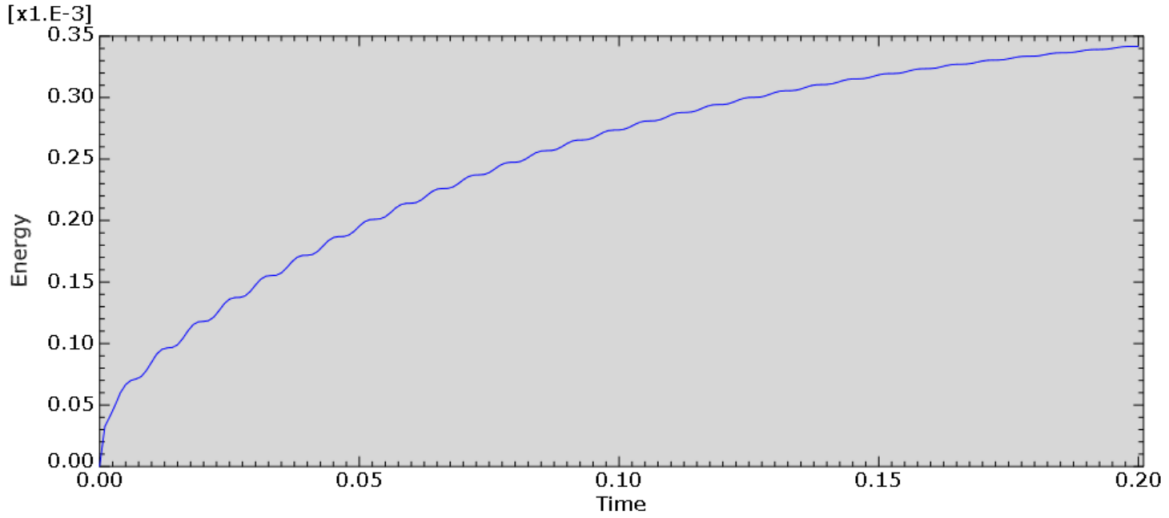
Figure 4.10: Viscous dissipation CAS model.
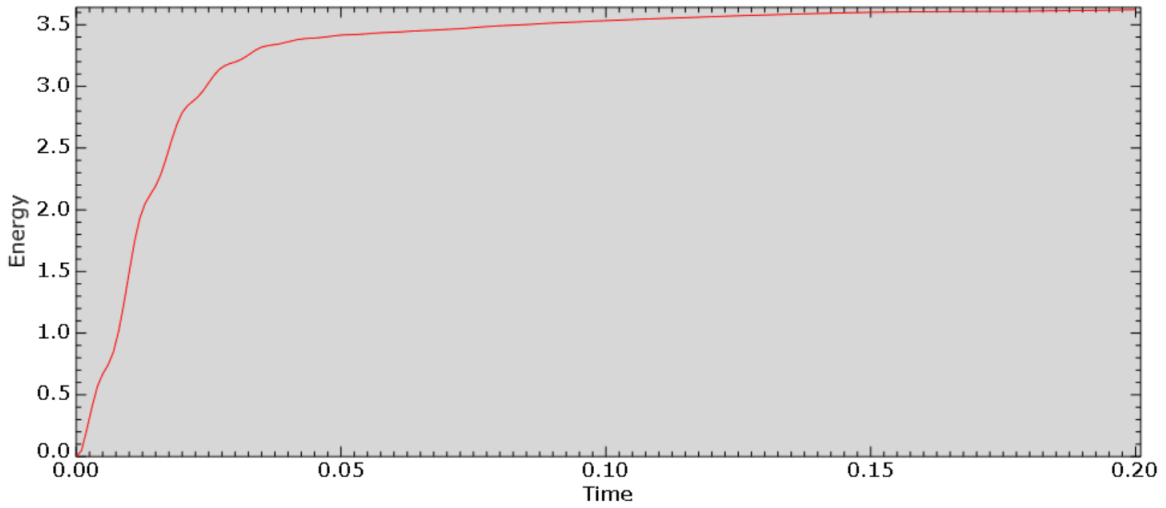
Figure 4.11: Viscous dissipation CEL model.

Figure 4.12 illustrates the viscous dissipation energies in a bar graph, and the fraction of viscous dissipation energy for the CAS analysis are very small in comparison to the CEL analysis The fraction of viscous dissipation energy for the CAS analysis, calculated in equation 4.3 and are only 0.0000756 or 0.00756% of the CEL analysis.

$$\frac{\sum dissipation_{CAS}}{\sum dissipation_{CEL}} = \frac{0.04994773mJ}{660.363005mJ} \approx 0.0000756 \tag{4.3}$$
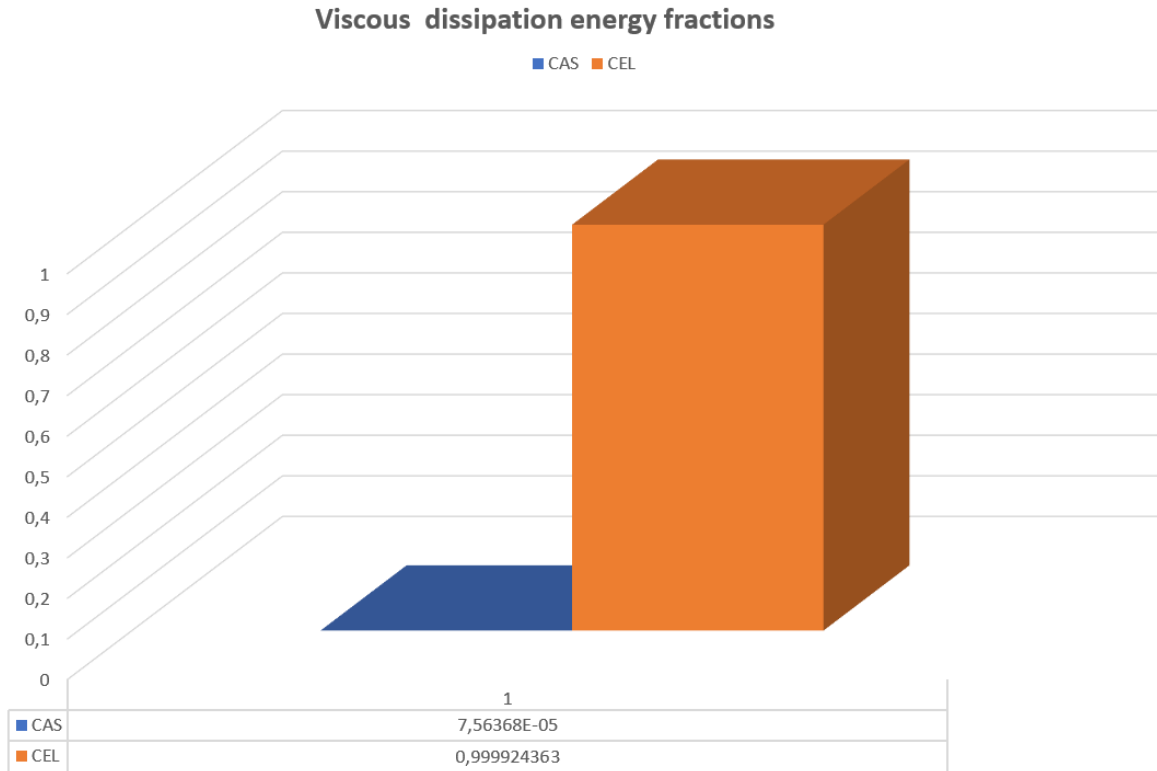
Figure 4.12: Viscous dissipation energy comparison.

4.5 Total energy

The total energy output, ETOTAL, can be used to see if the analysis are yielding a proper response. In table 4.2 the total energy output over the simulation period are presented for the CAS analysis and CEL analysis, to give the reader insight of the quantities involved.

In figure 4.13 for the CAS analysis a small change in total energy is observed as the instantaneous load is applied. The change may seem significant but observing the scale of the vertical axis gives an understanding of the small change. Almost no change in total energy can be observed afterwards, so it is approximately constant.

Figure 4.14 illustrates the total energy for the CEL analysis. A change in total energy is seen throughout the simulation which indicates that energy is "leaking" out of the model. By looking at this graph alone it would not pass a sanity test for acceptable finite element results. The result needs to be further investigated to see the bigger picture of the analysis. This will be done in the next section .

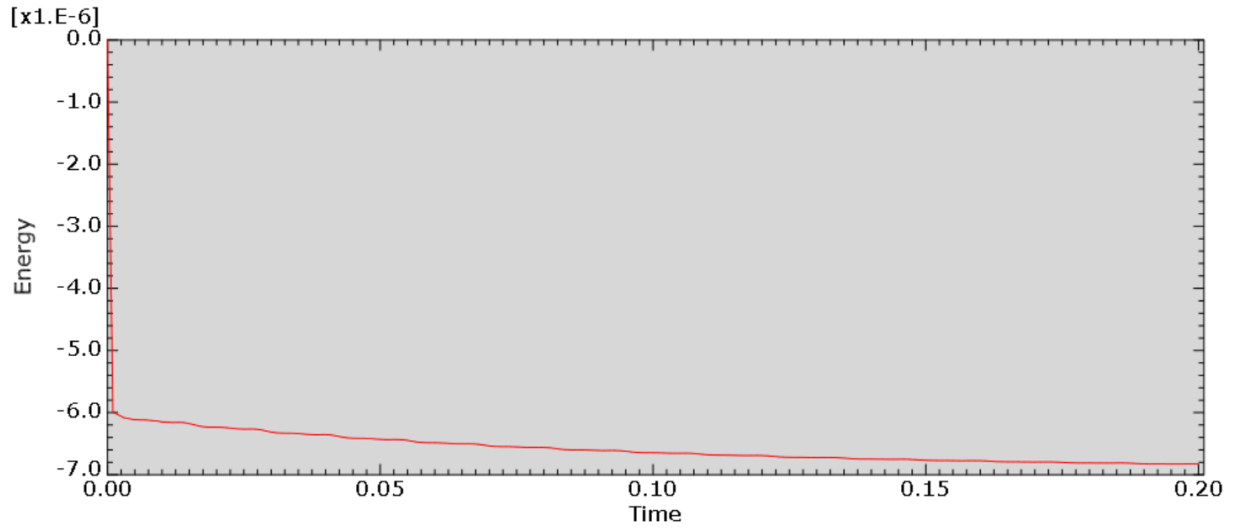| Analysis	Energy [mJ]
CAS	-0.0013
CEL	-132.5765

Table 4.2: Total energy.

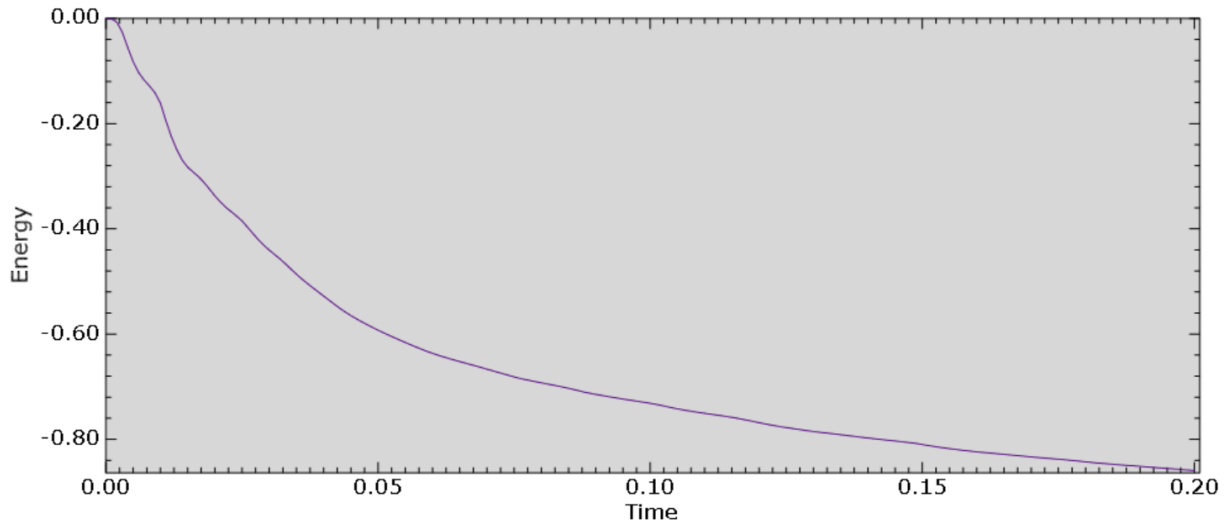Figure 4.13: Total energy CAS model.

Figure 4.14: Total energy CEL model.

4.6 Energy balance and variation

The energy balance principle was presented in equation 2.58, where the total energy should be equal to the sum of all energies taken into account. The total energy or sum of all energies should be constant throughout the simulation. For a numerical analysis this is not completely true. The total energy or sum of energies will vary throughout the simulation due to numerical errors, hour-glassing, non-linearity, energies not taken into account and general Abaqus capabilities. Instead of claiming the total energy or sum of energies should be constant, the variation of energies throughout the analysis will be investigated. The variation of energy will be used as a basis for a sanity check to control if the analysis are yielding a proper response.

For the CAS analysis figure 4.15 is a direct output of all energies considered. The total energy seems absolutely constant and zero compared to the other energies. The result is promising and indicates that the simulation is adequate. The frictional energy also seems to be zero from the plot, which it should be, as no friction forces are applied to the system. The viscous dissipation energy seems to follow the same path, but as observed from figure 4.10, this energy is not zero but very small. The kinetic energy is oscillating with a slow decay. The external work and internal energy follows the same oscillating path, also with a slow decay.
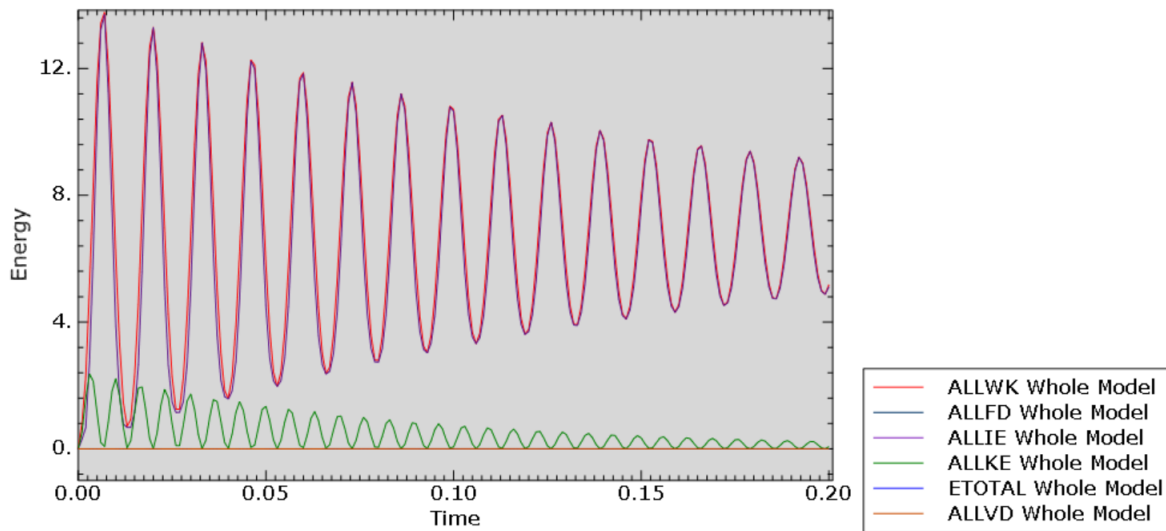

Figure 4.15: Energies CAS model.

By individually summing up all energies over the whole simulation period, an overview of how the quantities of energy are distributed to each of the energies taken into account, this can be seen in table 4.3. Calculation below shows an equal quantity of energy at both sides of the energy conservation equation. As these energy quantities are over the total simulation period, no variation will be calculated. Anyhow, the energy quantity on the left hand side and right hand side are equal, and the total energy is constant through the simulation, therefore it can now be assumed that the numerical analysis are yielding correct response.

$$ETOTAL = ALLIE + ALLVD + ALLFD + ALLKE - ALLWK$$

$$ETOTAL = \underbrace{1275.0823 + 0.0499 + 0 + 94.5729 - 1369.7064}_{-0.0013}$$

$$-0.0013 = -0.0013$$

Variable name	ALLWD	ALLFD	ALLIE	ALLKE	ETOTAL	ALLVD
Energy total [mJ]	1369.7064	0	1275.0823	94.5729	-0.0013	0.0499

Table 4.3: Energies CAS analysis.

In figure 4.16 a plot of the variation, total energy and sum of all energies are presented. Equation 4.4 are the basis for representation of the variation. The subscript (i) denotes the time increment and the variation can now be shown for each increment. For the record, variation is meant as the difference between the total energy and sum of all energies in each time increment. In the graph describing the variation in energy very small fluctuations around the zero line are observed, and the same fluctuations are seen in the graph describing the total energy. The small fluctuations are neglected and the total energy is close to constant after the instantaneous load is applied.

Using figure 4.15 to see the bigger picture and figure 4.16 for closer investigation, the results seems reasonable. In regards to a sanity check, it is therefore basis to claim that all results produced in the CAS analysis are correct with the given preconditions. But it is important to keep in mind that the preconditions in the CAS analysis might not be a good representation for a real situation.

$$VARIATION_{(i)} = ETOTAL_{(i)} - \left[ALLIE_{(i)} + ALLVD_{(i)} + ALLFD_{(i)} + ALLKE_{(i)} - ALLWK_{(i)} \right]$$
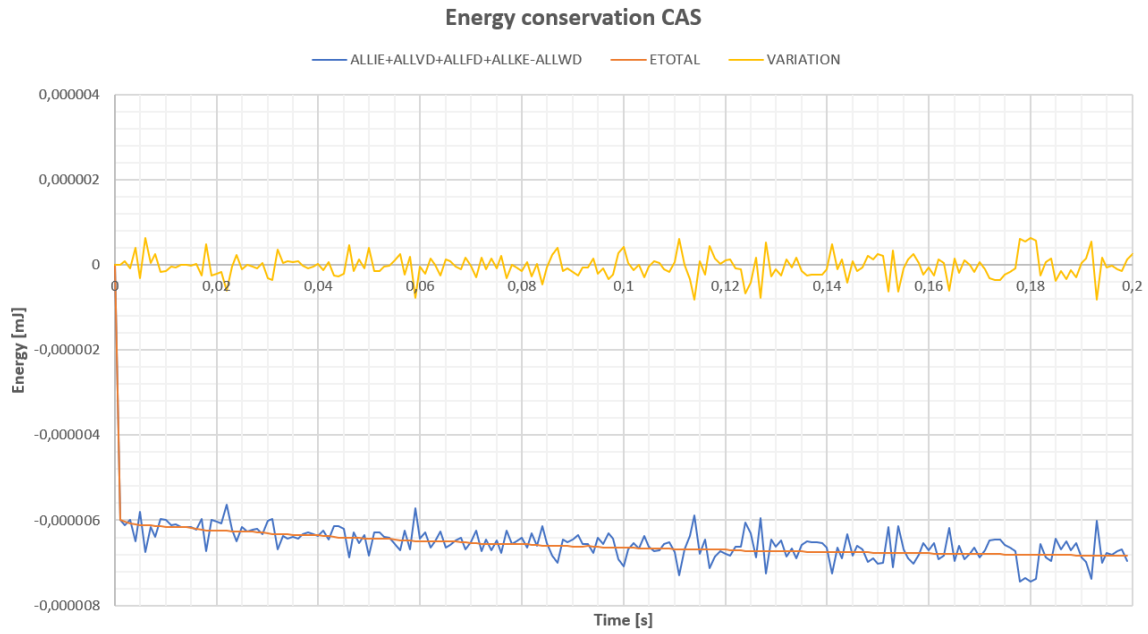
$$(4.4)$$

Figure 4.16: Energy and variation plot CAS.

For the CEL analysis, figure 4.17 is a direct output of the energies accounted for in the simulation. A frictionless behaviour was chosen for the model, and from the rough scale graph it also seems that no friction energy is present. The viscous energy dissipation was the energy dissipated by damping mechanisms. This portion is relatively large for the analysis so a lot of energy is used for damping. By inspecting the graph and from previous figure 4.11, it is clear that the viscous energy dissipation becomes almost constant after some time. This implies that the damping also becomes relative constant.

The internal energy oscillates in the same way as the work done by external forces oscillates, but does not overlap as in the CAS analysis due to the large portion of energy transferred to viscous dissipation energy. The kinetic energy has a rapid decay and becomes constant and close to zero as previously stated in the kinetic energy section 4.3.

In the graph for total energy it is clear that it is not constant in the first $0.05s$ of the simulation, but seems stabilized and approximated constant from $0.05s$ to $0.2s$ in the figure. The figure does provide a great perception of development of all the energies as they plotted together, but as previously observed in figure 4.14 it was clear that the total energy were not constant.

For a sanity check this is a case of doubt. Argument for a pass of the analysis would be that there are no sudden jumps in total energy, and that it seems almost constant and stable after $0.05s$ when compared to the other energies. Argument for discard of the analysis would be that it is not constant before $0.05s$ and is slightly "leaking" energy after. The reasons for the not constant total energy are probably the instantaneous force applied, and that the instant deflection of the structural domain might not have been captured perfectly by the Eulerian domain. Remembering that the Eulerian elements are fixed in space so there are no node to node contact between the domains.

The leakage of fluid through the structural domain might also be a contributor as well as the transition from smaller to bigger elements in the Eulerian domain. The leakage problem are a well known problem for CEL analysis and may be improved by smaller element size for the part acting as a sieve. A finer mesh, with no transition to courser mesh, should have been applied to the whole model and probably limited some of the leakage of energy issue.

The boundary conditions may also have an influence on the energy leakage, even if at this point there is no evidence for such an allegation. But it is experienced that the boundary conditions does influence the damping effect and therefore the viscous dissipation energy. In general, CEL analysis are known to have a reduced accuracy compared to other analysis.
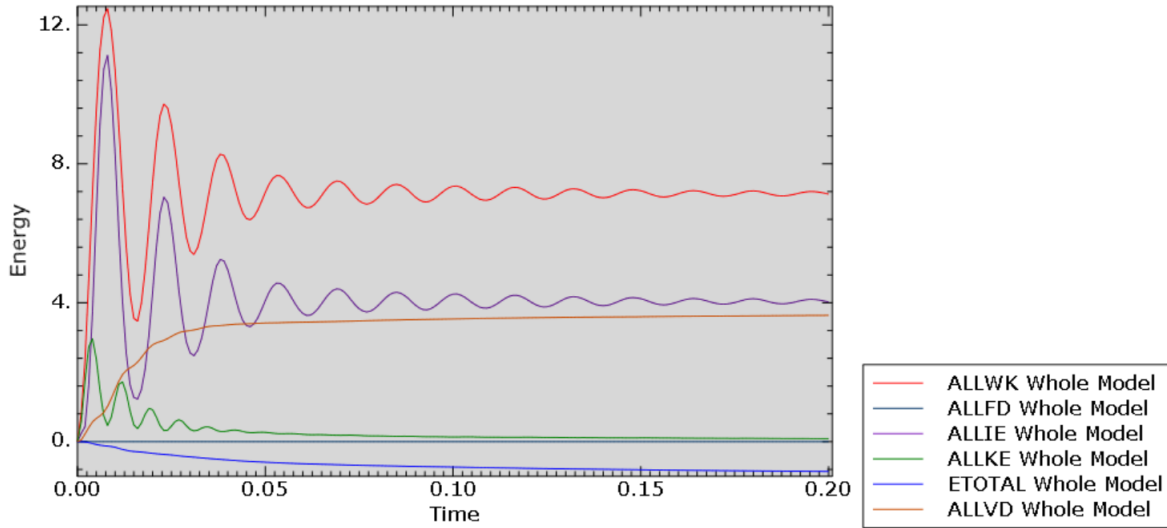
Figure 4.17: Energies CEL model.

Each of the energy quantities are summed up over the total simulation period in table 4.4. This is to provide an impression of where the energy quantities are distributed. In equation below, the total energy are on the left hand side and summation of all other energies on the right hand side. The left and right hand side does not add up which indicates that it is a problem with the simulation or model.

$$ETOTAL = ALLIE + ALLVD + ALLFD + ALLKE - ALLWK$$

$$ETOTAL = \underbrace{825.7416 + 660.3630 + 0 + 55.1435 - 1431.9414}_{109.3067}$$

$$-132.3423 \neq 109.3067$$

Variable name	ALLWD	ALLFD	ALLIE	ALLKE	ETOTAL	ALLVD
Energy [mJ]	1431.9414	0	825.7416	55.1435	-132.3423	660.3630

Table 4.4: Energies CEL analysis.

Figure 4.18 provides a comparison of the total energy, sum of all energies and variations. Also here it is worth notice that the variations are meant as the difference between the total energy and the sum of all energies, so equation 4.4 are still the basis, where the variation is for each time increment. A relative stable but big variation can be observed, also approximated constant from $0.05s$. This indicated that the main issues in the simulation are at the beginning of the simulation.

For the question of the sanity of the analysis it is still a case of doubt, but for engineering purposes of the results, recommendation would be to discard the analysis. The total energy must be very close to constant to ensure perfect results. That being said, the purpose of this master thesis was to investigate whether the CEL technique was implementable on immersed structures, which it has been proven to be.
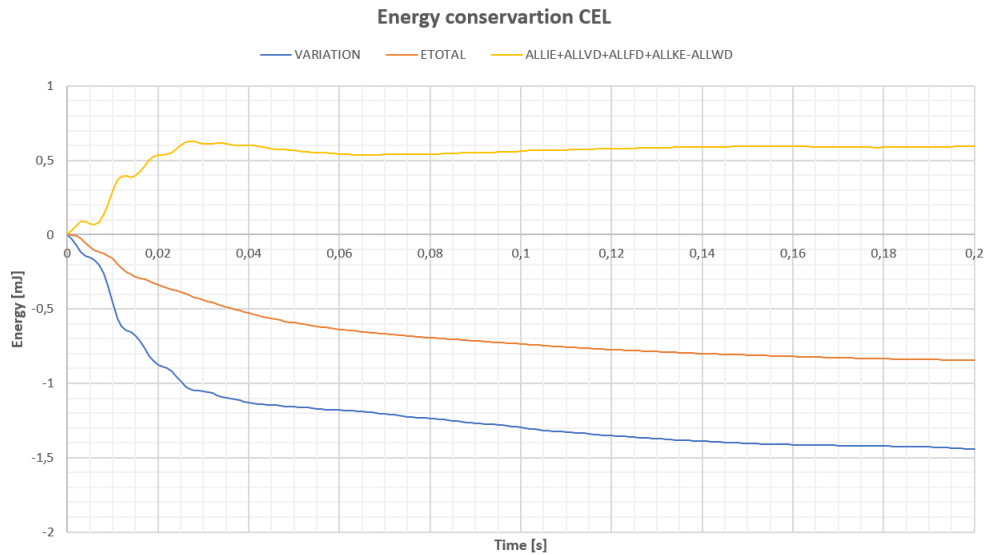

Figure 4.18: Energy and variation plot CEL.

5 Conclusion

The two numerical analysis methods presented in the master thesis have very different approaches for the FSI problem. Both methods are implementable and good approaches for the problem with a structure immersed in a fluid. However the results in the CAS analysis are sprawling compared to the CEL analysis due to the different preconditions in the model setup. The CAS analysis should have been provided with an acoustic impedance and/or drag force to replicate the viscosity in the CEL analysis. But implementing such parameters are difficult and probably not yield desired response.

On basis of the different preconditions for the two numerical analysis, a damping ratio of $\zeta_{CAS} = 1.1\%$ for the CAS analysis and a damping ratio of $\zeta_{CEL} = 7.1\%$ for the CEL analysis, are calculated for the submerged structures. In lack of experimental results it is impossible to determine which is most appropriate, but experience would suggest that the CEL analysis is closest to reality. The added viscosity in the CEL analysis are definitely the main contributor to the damping effect. As the damping ratios are calculated from the displacements, the displacements for the CEL analysis tends to decay faster then for the CAS analysis. The same does also apply to the velocities.

In the energy aspect for the two analysis, table 4.3 and 4.4 shows how the energy quantities are distributed in the simulation period of $0.2s$. A larger quantity of energy is reserved for the damping mechanisms in the CEL analysis than in the CAS analysis, i.e the viscous dissipation energy. This is also related to the values of damping ratios.

The total energy in the CAS analysis are approximated constant throughout the simulation and therefore it can be concluded that all results are reliable with the given preconditions. The total energy in the CEL analysis are seen not to be constant throughout the simulation and the results are recommended to be discarded. This might be a strict decision or even incorrect, but decision is based in the change of total energy from $0s$ to $0.05s$.

However, one of the main reasons with this master thesis was to investigate whether the CEL technique was suitable for this type of problem. Without doubt it is very suitable. Issues regarding the change in total energy can most likely be bypassed by refining the mesh, no mesh transitions and apply the load in a different manner.

Overall both simulation techniques are suitable for this kind of problem, despite the issues with the total energy and the complex setup, the CEL technique is the preferred numerical method. This method can be provided to a larger variety of problems, such as a moving fluid. A convergence study should also have been implemented for both methods for optimizing the choice of mesh size and therefore simulation time.

6 Further Work

The simplified model of a Francis turbine used in this master thesis has shown that both CAS technique and CEL technique can be used for this type of problems. The lack of experimental results has been a drawback, so it is highly recommended to obtain experimental results. With experimental results it would be much easier to determine which type of simulation that provides the best results compared to model setup effort. The numerical model must be redesigned to fit a model available to do experiments on, or a experimental model must be created to verify or discharge results obtained in this master thesis. Procedures of model setup are well described in appendix A and appendix C, so a new model build up should be possible. A refinement of the meshes are highly recommended.

It is also recommended to study and implement the analysis performed in signatory's specialization project [30] to the model available for experimental results. These simulations gives a foundation for understanding the Abaqus software and the complexity of the physical problem.

References

[1] A.Craggs. The transient response of a coupled plate-acoustic system using plate and acoustic finite elements. *Sound vibrations*, pages 509–528, 1970.

[2] G.C Everstine. Finite element formulation of structural acoustic problems. *Computers and structures*, 65:307–321, 1995.

[3] Peter Davisdon Gøran Sanberg, Per-Andreas Wernberg. Fundamentals of fluid-structure ineraction. *CISM International Centre for Mechanical Sciences, Courses and Lectures*, pages 23–101, 2009.

[4] Roger Ohayen Gøran Sandberg. *Computational Aspects of Structural Acoustics and Vibration*. Springer Vienna, Springer Heidelberg Dordrecht London New York, 1 edition, 2009. ISBN : 1-282-33282-1.

[5] Simulia. Abaqus analysis user's manual: 6.10.1:acoustic, shock and coupled acoustic-structural analysis: Load. https://www.sharcnet.ca/Software/Abaqus610/Documentation/docs/v6.10/books/usb/default.htm?startat=pt07ch30s04aus113.html, 2017. [online; 29.april 2019].

[6] D.J. Beson. Computational methods in lagrangian and eulerian hydrocodes. *Computer Methhods in Applied Mechanics and Engineering*, pages 235–394, 1992.

[7] S.Okazawa D.J. Benson. Contact in a multi-material eulerian finite element formulation. *Computer methods in applied mechanics and engieering*, pages 4277–4298, 2004.

[8] K.J. Bathe S.Rugonyi. On finite element analysis of fluid flows fully coupled with structural interactions. *CMES*, pages 195–212, 2001.

[9] Dassault Systèmes. Eulerian analysis. https://www.sharcnet.ca/Software/Abaqus/6.14.2/v6.14/books/usb/default.htm?startat=pt04ch14s01aus90.html, 2016. [online; 5.mars 2019].

[10] P. Bettess O.C Zienkiewicz. Fluid structure dynamic interaction and wave forces. an introduction to numerical treatment. *International journal for numerical methods in engineering,* pages 1–16, 1978.

[11] Ted Belytschko Jacob Fish. *A first Course in Finite Elements.* Wiley, The Atrium, Southern Gate, Chichester, West Sussex PO19 8SQ, England, 1 edition, 2007. ISBN : 978-0-470-03580-1.

[12] Hans Petersson Niels Ottosen. *Introduction to the Finite Element Method.* Pearson, Prentice Hall Europe, Edinbirgh Gate, Harlow,Essex CM20 2JE,England, 1 edition, 1992. ISBN-13 : 978-0-13-473877-2.

[13] Wikipedia. Lamè parameters. https://en.wikipedia.org/wiki/Lamè_parameters, 2018. [online; 1.mars 2019].

[14] Dassault Systèmes. Acoustic medium. https://www.sharcnet.ca/Software/Abaqus/6.14.2/v6.14/books/usb/default.htm?startat=pt05ch26s03abm58.html, 2016. [online; 28.feb 2019].

[15] Simens PLM. Acoustics user guide. https://docs.plm.automation.siemens.com/data_services/resources/nxnastran/11/help/tdoc/en_US/pdf/acoustic.pdf, 2016. [online; 4.mars 2019].

[16] Ted Belytschko. Methods and programs for analysis of fluid-structure systems. *Nuclear engineering and design 42,* pages 41–52, 1977.

[17] T.K. Zimmermann T.J.R. Hughes, W.K Liu. Lagrangian-eulerian finite element formulations for incompressible flows. *Computer methods in applied mechanics and engieering,* pages 329–349, 1981.

[18] S.Giuliani J.Donea, P.Fasoli-Stella. Lagrangian and eulerian finite element techniques for transient fluid-structure interaction problems. *Computer Methods in Applied Mechanics and Engieering,* pages 1–12, 1977.

[19] R.A. Sauer K.K. Mandapu A. Sahu, Y.A.D. Omar. Arbitrary lagrangian-eulerian finite element method for curved and deforming surfaces. *General theory and application to fluid interfaces,* pages 1–63, 1981.

[20] Wikipedia. Logarithmic decrement. https://en.wikipedia.org/wiki/Logarithmic_decrement, 2019. [online; 4.april 2019].

[21] Clarence W. de Silva. *Vibration And Shock Handbook.* Tyler and Francis, Boca Raton, 1 edition, 2005. ISBN : 978-084-931-5800.

[22] Dassault Systèmes. Conversion tables, constants, and material properties. https://www.sharcnet.ca/Software/Abaqus/6.14.2/v6.14/books/popups/usb-tbl.html, 2016. [online; 8.april 2019].

[23] Abaqus Inc. Abaqus explicit advanced topics. https://imechanica.org/files/0-overview%20Explicit.pdf, 2005. [online; 23.april 2019].

[24] Simulia. Abaqus theory guide: Energy balance. http://130.149.89.49:2080/v6.14/books/stm/default.htm?startat=ch01s05ath12.html, 2017. [online; 23.april 2019].

[25] Simulia. Interactive edition: Energy balance. https://www.sharcnet.ca/Software/Abaqus/6.14.2/v6.14/books/gsa/default.htm?startat=ch09s06.html, 2017. [online; 23.april 2019].

[26] Dassault Systèmes. Explicit dynamic analysis. https://www.sharcnet.ca/Software/Abaqus610/Documentation/docs/v6.10/books/usb/default.htm?startat=pt03ch06s03at08.html, 2016. [online; 25.mars 2019].

[27] Jame Shau-Jen Ong Ted Belytschko. Hourglass controll in linear and non linear problems. *Computer Methhods in Applied Mechanics and Engineering,* 43:251–276, 1984.

[28] Dassault Systèmes. The voulme fraction tool. https://www.sharcnet.ca/Software/Abaqus610/Documentation/docs/v6.10/books/usi/default.htm?startat=pt04ch27s05.html, 2017. [online; 25.mars 2019].

[29] Woo Il Lee Min Soo Kim. A new vof-based numerical scheme for the simulation of fluid flow with free surface. part i: New free surface-tracking algorithm and its verification. *International journal for numerical methods in fluids*, 42:765–790, 2003.

[30] Frank Hanekamhaug. Dynamic eigenvalue analysis of a high head francis turbine. *Specialization project*, pages 1–28, 2018.

Appendix A   CAS model setup

Geometries and properties for the structural and acoustic domains are to be found in table 3.1 and table 3.2. The parts need to be created with given dimensions in the **part module**. A space equal to the dimension of the structural geometry need to be created inside the acoustic geometry using the create cut and extrude. It is wise to create datum planes off-centered $\pm 2.5mm$ from the principle xz-plane to create the cut. Alternatively the merge/cut instances in the **assembly module**. This feature is recommended for fit of more complex models. A reference point is also created in the center of both parts. The structural geometry must be partitioned on the top face to ensure that a node will be placed where the concentrated load is applied.

In the **property module** all the material properties are applied to each of the parts, in addition an acoustic interface is created under create section. This feature will automatically be set to the correct region when later applying the tie constraints. In the **assembly module** both parts are mounted so the structural geometry is centered inside the acoustic geometry. Now the reference points are used for translating or rotating the geometries to the correct position.

The **mesh module** is then opened and the structural geometry is selected. This part is given global seeds of 5mm and local seeds of 2.5 mm in the height, i.e y-direction. Elements of type C3D8R are assigned, and the mesh control used to ensure that only hexahedral elements are applied. Then mesh the part. The acoustic geometry is then ready to be meshed, and applied hexahedral elements. Some partitioning must be done to make the model ready for the hexahedral mesh. Use the toolbar to create more datum planes, $\pm 12.5mm$ off centered from the principle xz-plane and $\pm 100mm$ from the yz-plane. Use these datum planes to partition the part. Note that the same partitioning can be obtained using other approaches. The acoustic geometry is now ready to be assigned hexahedral elements of type AC3D8R. Global seeds of 10 mm, and local seeds of 2.5 mm in the y-direction region between the $\pm 12.5mm$ partitioning is done. This is to ensure smaller mesh in the contact and interesting regions. See figure A.1 for complete partitioning of the models.

Interaction module is then opened and tie constraints are applied. All surface regions of the structural geometry are chosen to be the master surface, and the created space inside the acoustic geometry is the slave surface. Due to the meshing, the nodes in both surfaces should now be coincide in the y-direction, so the default options for position tolerance is chosen to complete the tie constraint feature. A planar, non-reflecting acoustic impedance interaction is also created at all outer surfaces of the acoustic medium. This is an assumption and prevents acoustic waves reflecting back and forth inside the medium creating noise. Next is to create a dynamic explicit step in the **step module**, a time period of 0.2 seconds is chosen to be appropriate and all other parameters stays as default options.

Load module is then opened and a boundary condition type encastre is chosen and applied at the end surface of the structural geometry. The boundary condition holds the geometry fixed in all direction at the end. It is wise to apply this as an initial condition in case of later changes to the model. A concentrated instantaneous force of 10 N is applied to the geometry in the negative y-direction. The force is centered 10 mm from the tip of the steel plate.

A job is created in the **job module**, with a double precision output only for the analysis, and use of multiple processors for faster analysis. From the model tree a new history output is created for the point where the load is applied. A displacement/velocity/acceleration history output for this point is set to be 500 points during the analysis period. The job are then ready to be submitted.

When the job is completed, the **visualization module** is used for visual control and inspection of the dynamic behaviour of the model. See figure A.2.
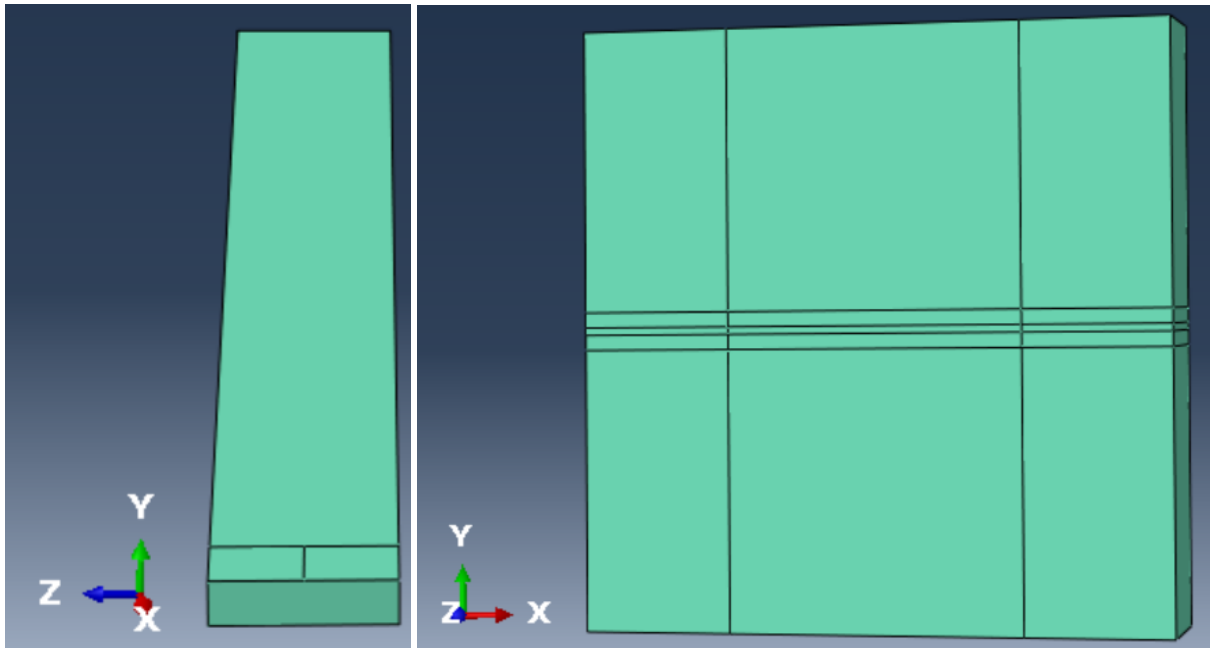
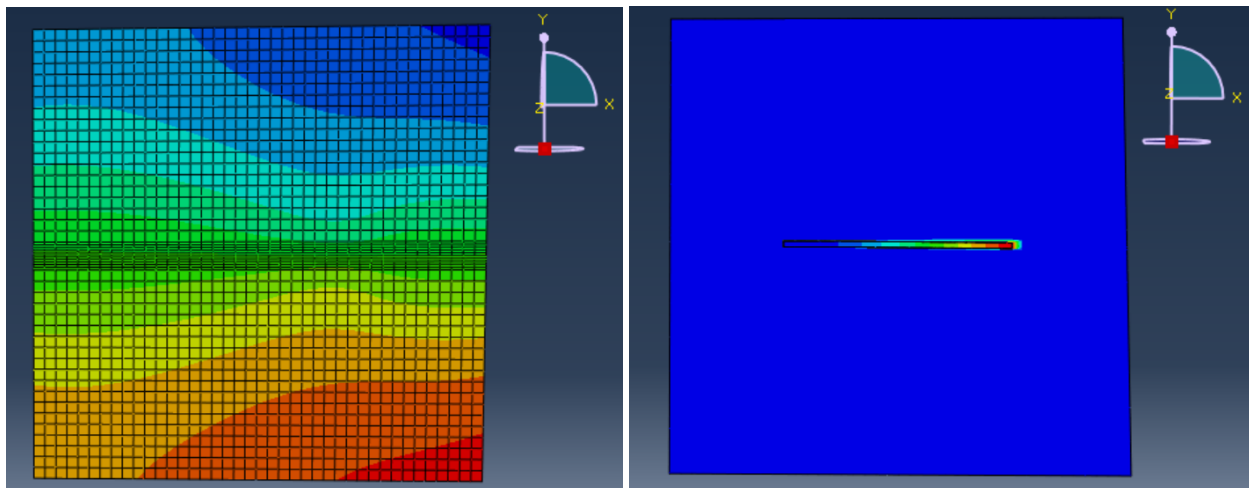Figure A.1: Geometry and partitioning CAS analysis.

Figure A.2: Acoustic pressure for control and dynamics.

Appendix B　CAS simulation input file

```
*Heading
** Job name: expMAST Model name: Model-1
** Generated by: Abaqus/CAE 2017
*Preprint, echo=NO, model=NO, history=NO, contact=NO
----------------------------------------------------------
** PARTS
**
*Part, name=beam
*Element, type=C3D8R
*Part, name=medi
*Element, type=AC3D8R
----------------------------------------------------------
** ASSEMBLY
**
*Instance, name=beam-1, part=beam
*Instance, name=medi-1, part=medi
** Constraint: TIED
*Tie, name=TIED, adjust=yes
----------------------------------------------------------
** MATERIALS
**
*Material, name=medivann
*Acoustic Medium
2200.,
*Density
 1e-09,
*Material, name=steel
*Density
```

```
 7.85e-09,
*Elastic
200000., 0.3
*Time Points, name=TimePoints-1, GENERATE
0., 0.2, 0.0001
----------------------------------------------------------
** BOUNDARY CONDITIONS
**
** Name: fixed Type: Symmetry/Antisymmetry/Encastre
*Boundary
Set-2-fixed, ENCASTRE
----------------------------------------------------------
** STEP: expMASTER
**
*Step, name=expMASTER, nlgeom=YES
*Dynamic, Explicit
, 0.2
*Bulk Viscosity
0.06, 1.2
----------------------------------------------------------
** LOADS
**
** Name: force10mm   Type: Concentrated force
*Cload
Set-6-kraften10mm, 2, -10.
----------------------------------------------------------
** INTERACTIONS
**
** Interaction: Int-1-PLANARIMP
*Simpedance, nonreflecting=PLANAR
```

```
Surf-4-planIMP

-------------------------------------------------------

** OUTPUT REQUESTS

**

*Restart, write, number interval=1, time marks=NO

**

** FIELD OUTPUT: F-Output-1

**

*Output, field, number interval=200

*Node Output

A, PABS, POR, RF, U, V

*Element Output, directions=YES

CTSHR, EVF, LE, MISES, MISESMAX, MISESONLY, PE, PEEQ, PEEQVAVG, PEVAVG, PRESSONLY, PS, S

TRIAX, TSHR, VS

*Contact Output

CSTRESS,

**

** FIELD OUTPUT: F-Output-2

**

*Node Output

A, PABS, POR, RF, U, V

*Element Output, directions=YES

EDCDEN, EDT, ELEDEN, ELEN, ENER, EVF, LE, PE, PEEQ, PEEQVAVG, PEVAVG, S, SVAVG

*Contact Output

CSTRESS,

**

** HISTORY OUTPUT: H-Output-1

**

*Output, history, variable=PRESELECT, frequency=200

**
```

```
** HISTORY OUTPUT: H-Output-2
**
*Output, history, time interval=0.0004
*Node Output, nset=Set-5-forceTIP
A1, A2, A3, AR, AR1, AR2, AR3, AT
CF1, CF2, CF3, CM1, CM2, CM3, RF1, RF2
RF3, RM, RM1, RM2, RM3, RT, RWM, U1
U2, U3, UR, UR1, UR2, UR3, UT, V1
V2, V3, VR, VR1, VR2, VR3, VT
**
** HISTORY OUTPUT: H-Output-3-U10mm
**
*Node Output, nset=Set-6-kraften10mm
A1, A2, A3, AR, AR1, AR2, AR3, AT
U1, U2, U3, UR, UR1, UR2, UR3, UT
V1, V2, V3, VR, VR1, VR2, VR3, VT
```

Appendix C CEL model setup

The geometries for the structural geometry, Eulerian geometry and the dummy container geometry are created in the **part module** with dimensions given in table 3.1 and table 3.4. The dummy container and the Eulerian domain have the same dimensions, due to the fact that the Eulerian properties are going to be filled inside the dummy container and this is the only region of interest. The dummy container must be created as a discrete rigid type. A space equal to the dimensions of the structural geometry is created centered inside the dummy container. This is done by creating datum planes off centered $\pm 2.5mm$ from the principle xz-plane, and use the create cut and extrude feature.

The rigid dummy container must be transformed from a solid to a shell. This option is found in the tool bar. Reference points are created for all three parts in the center of each of them. The structural geometry is partitioned at the top face to ensure that a node will be placed where the load is going to be applied. The Eulerian domain is also partitioned at all faces $\pm 12.5mm$ off centered from the principle xz-plane. The dummy container undergoes the same partitioning. Se figure C.1.

In the **property module** the structural geometry and Eulerian geometry are assigned properties from table 3.1 and table 3.4, while the dummy are not assigned any properties. The parts are then ready to be meshed in the **mesh module**. The structural geometry is assigned hexahedral elements, global seeding of 5mm and local seeding of 2.5 mm in the y-direction, then meshed with C3D8R type elements. The Eulerian geometry is assigned global seeds of 10 mm and local seeds of 2.5 mm in y-direction in the region partitioned $\pm 12.5mm$ from the xz-plane. Hexahedral mesh of type EC3D8R is then applied. The dummy is assigned global seeds of 10 mm, and 2.5 mm in y-direction in the same region as the Eulerian. Since the dummy is a shell, local seeds of 2.5 mm in y-direction must be applied to the space inside where the structural geometry is to be mounted. This completes the meshing.

The **interaction module** must now be opened and from the toolbar the discrete field–>volume fraction tool is found. Selecting the Eulerian, and then the dummy container as the reference part, to begin the filling of the volume. Filling accuracy is chosen to high, and a node set and element set is selected to be created. Now the volume is filled but it is crucial to assign the material it is filled with. Open the **load module**, go to predefined field, choose "other" and material assignment. Choose the Eulerian part instance and the edit predefined field opens, choose the discrete field definition to assign the material.

In the **step module** a dynamic explicit step can now be created with time period of 0.2 s. All options stays as default. Go back to the **interaction module** and create interaction property. This is set to be frictionless tangential behaviour and hard contact normal behavior. Go to the interaction manager and apply general contact to all surfaces. This becomes the only contact between the structural domain and the Eulerian domain, since dummy is going to be suppressed.

In the **load module**, encastre boundary conditions are applied to the end surface of the structural geometry. At the outer surfaces of the Eulerian geometry, an Eulerian boundary condition is applied. This is set to be free inflow and non-reflecting outflow. This assumption will prevent the fluid from reflecting back and forth in the domain and produce vibrations. The instantaneous concentrated force of 10 N is applied to the centred node 10 mm from the tip of the structural geometry. A displacement/velocity/acceleration history output are created for the node, and set to 500 points during the analysis. Now suppress the dummy container.

In the **job module** a job is created, with double precision only for analysis and use of multiple processors for speeding up the analysis. The job is now ready to be submitted. When the job is completed the **visualization module** provides a wide variety of visual effects. See figure C.2 and figure C.3.
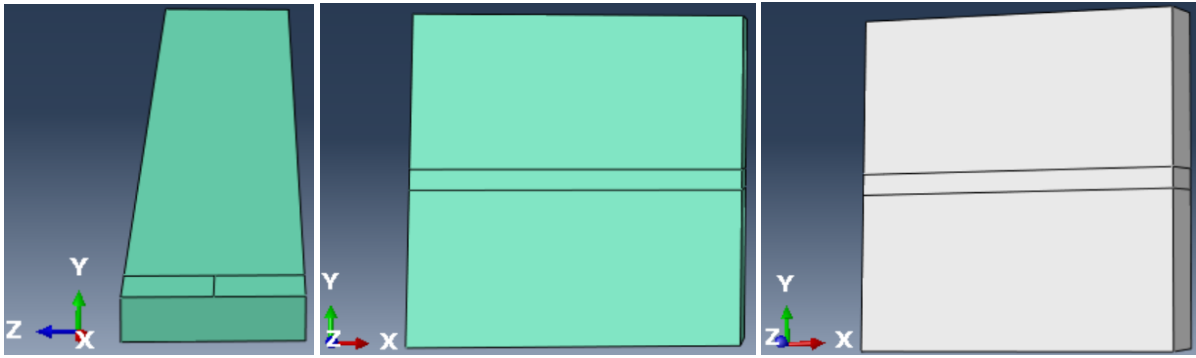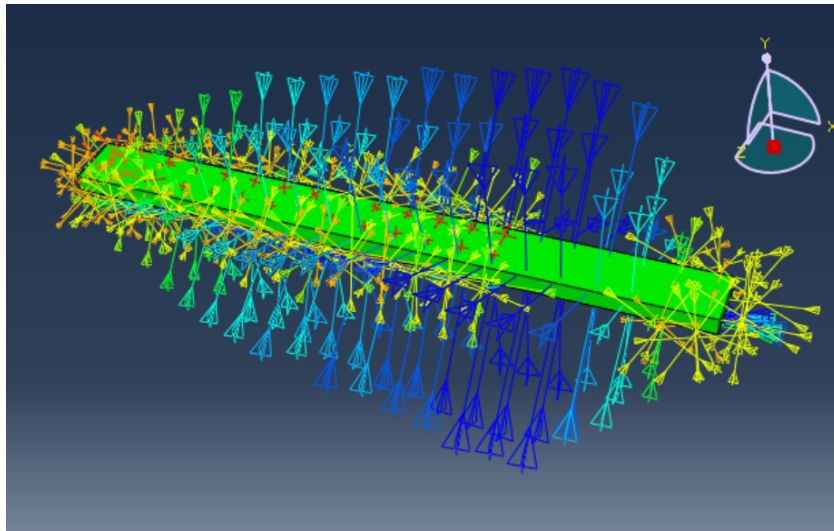
Figure C.1: Geometry and partitioning CEL analysis.

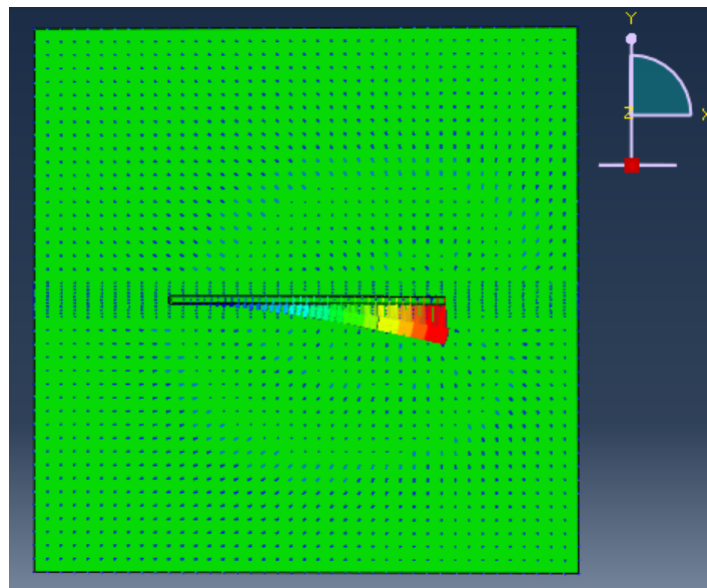

Figure C.2: Volume fraction averaged stress.

Figure C.3: Vectors illustrating displacements.

Appendix D   CEL simulation input file

```
*Heading
** Job name: expEULdisplace Model name: Model-1
** Generated by: Abaqus/CAE 2017
*Preprint, echo=NO, model=NO, history=NO, contact=NO
-------------------------------------------
** PARTS
**
*Part, name=Beam
*Element, type=C3D8R
*Part, name=EUL
*Element, type=EC3D8R
-------------------------------------------
** ASSEMBLY
**
*Instance, name=Beam-1, part=Beam
*Instance, name=EUL-1, part=EUL
-------------------------------------------
** MATERIALS
**
*Material, name=steel
*Density
 7.85e-09,
*Elastic
200000., 0.3
*Material, name=water
*Density
 1e-09,
*Eos, type=USUP
```

```
  1.5e+06,0.,0.
*Viscosity
 1e-09,
-----------------------------------------------
** INTERACTION PROPERTIES
**
*Surface Interaction, name=IntProp-1
*Friction
0.,
*Surface Behavior, pressure-overclosure=HARD
** INTERACTIONS
**
** Interaction: Int-1
*Contact, op=NEW
*Contact Inclusions, ALL EXTERIOR
*Contact Property Assignment
 ,  , IntProp-1
-----------------------------------------------
** BOUNDARY CONDITIONS
**
** Name: fixed Type: Symmetry/Antisymmetry/Encastre
*Boundary
Set-4, ENCASTRE
** BOUNDARY CONDITIONS
**
** Name: BC-5-EULBOUND Type: Eulerian boundary
*Eulerian Boundary, inflow=FREE, outflow=NONREFLECTING
Surf-1-EulBOUNARYnr
-----------------------------------------------
** PREDEFINED FIELDS
```

```
**
** Name: Predefined Field-1   Type: Material assignment
*Initial Conditions, type=VOLUME FRACTION
---------------------------------------------
** STEP: expEULERIANdisp
**
*Step, name=expEULERIANdisp, nlgeom=YES
*Dynamic, Explicit
, 0.2
*Bulk Viscosity
0.06, 1.2
---------------------------------------------
** LOADS
**
** Name: Load-1-force10mm   Type: Concentrated force
*Cload
Set-8, 2, -10.
---------------------------------------------
** OUTPUT REQUESTS
**
*Restart, write, number interval=1, time marks=NO
**
** FIELD OUTPUT: F-Output-1
**
*Output, field, variable=PRESELECT, number interval=200
**
** HISTORY OUTPUT: H-Output-1
**
*Output, history, variable=PRESELECT
**
```

```
** HISTORY OUTPUT: H-Output-3-tip
**
*Output, history, time interval=0.0004
*Node Output, nset=Beam-1.Set-2-tip
A1, A2, A3, AR, AR1, AR2, AR3, AT
U1, U2, U3, UR, UR1, UR2, UR3, UT
V1, V2, V3, VR, VR1, VR2, VR3, VT
**
** HISTORY OUTPUT: H-Output-2-Uforce
**
*Node Output, nset=Set-8
A1, A2, A3, AR, AR1, AR2, AR3, AT
U1, U2, U3, UR, UR1, UR2, UR3, UT
V1, V2, V3, VR, VR1, VR2, VR3, VT
```